

## Ultrafast Spectroscopy and Technological Application of Light Harvesting Nanomaterials

SOUMIK SARKAR, ABHINANDAN MAKHAL AND SAMIR KUMAR PAL

---

### ABSTRACT

In this article, we will review our investigation on the key ultrafast processes in the light harvesting dynamics of Zinc Oxide (ZnO)-based nanomaterials. Firstly, we describe our studies on light harvesting of the complex of ZnO nanoparticles (NPs) with biological probe Oxazine 1 in the near-infrared region using time-resolved second-resolved fluorescence decay studies. We have used ZnO NPs and Oxazine 1 as model donor and acceptor respectively to explore the efficacy of the Förster resonance energy transfer (FRET) in the nanoparticle-dye system. It has been shown that FRET from the states localized near the surface and those in the bulk of the ZnO NPs can be resolved by measuring the resonance efficiency for various wavelengths of the emission spectrum. It has been observed that the states located near the surface for the NPs (contributing to visible emission at  $\lambda \approx 550$  nm) can contribute to very high efficiency (>90%) FRET. The efficiency of light harvesting dynamics of the ZnO nanorods (NRs) has also been explored in this study and they were found to have much less efficiency (~40%) for energy transfer compared to the NPs. The possibility of electron transfer reaction has been ruled out from the picosecond-resolved fluorescence decay of the acceptor dye at the ZnO surface. Secondly, we report the dynamics of light harvesting of ZnO NPs to a surface adsorbed sensitizing dye (SD) N719 (Di-tetrabutylammonium cis-bis(isothiocyanato)bis(2,2'-bipyridyl-4,4'-dicarboxylato)ruthenium(II)). By using picoseconds-resolved FRET technique we have explored that the excited ZnO NPs resonantly transfer visible optical radiation to the SD N719. The consequence of the energy transfer on the performance of the overall efficiency of a model ZnO NP-

---

Department of Chemical, Biological and Macromolecular Sciences, S. N. Bose National Centre for Basic Sciences, Block JD, Sector III, Salt Lake, Kolkata 700 098, India  
\*Corresponding author: Email: skpal@bose.res.in (S. K. Pal)

based dye sensitized solar cell (DSSC) has also been explored. We have demonstrated that the overall efficiency of a ZnO NP-based solar cell significantly depends on the presence of high energy photons in the solar radiation. In a control experiment on a model TiO<sub>2</sub> NP-based solar cell, it has been demonstrated that the presence of high energy photon has minimal effect on the performance of the cell as the TiO<sub>2</sub> NPs are incapable of harvesting high energy photons from solar radiation. The possibility of the back electron transfer from the excited NPs to the SD has also been investigated by studying the NPs in presence of an ideal electron accepting organic molecule, benzoquinone (BQ). The time constants and nonradiative rate constant obtained for ZnO/N719 system found to be different from the ZnO/BQ system which rules out the possibility of back electron transfer from ZnO NPs to SD N719. Moreover, the observed FRET dynamics in the light harvesting process of the nanocrystalites may be efficient in the further use of the NPs in the development of new photodevices. Finally, we illustrate the photo-dependent exciton mechanism and the charge migration kinetics in a colloidal ZnO–Au NC system. By using a picosecond-resolved FRET technique, we have demonstrated that excited ZnO NPs resonantly transfer visible optical radiation to the Au NPs, and the quenching of defect-mediated visible emission depends solely on the excitation level of the semiconductor. The role of the gold layer in promoting photolytic charge transfer, the activity of which is dependent upon the degree of excitation, was probed using methylene blue (MB) reduction at the semiconductor interface. Incident photon-to-current efficiency measurements show improved charge injection from SD to semiconductor electrode in the presence of gold in the visible region. Furthermore, the short-circuit current density and the energy conversion efficiency of the ZnO–Au NP based DSSCs are much higher than a DSSC comprised of only ZnO NPs. Our results represent a new paradigm for understanding the mechanism of defect-state passivation and photolytic activity of the metal component in metal–semiconductor nanocomposite systems.

**Key words:** Nanocomposites, Dye sensitized solar cell (DSSC), FRET, Sensitizing dye (SD)

---

## 1. INTRODUCTION

An efficient light-harvesting step is critical for the success of various biologically important processes including photosynthesis, where rapid excitation energy transfer from the outer antenna to the reaction centre is required to compete with normal excited-state quenching<sup>[1]</sup>. However, the precise molecular principles that enable such high efficiency have remained elusive because of the lack of both experimental and theoretical tools that can unambiguously reveal coupling and dynamics of the multi-chromophoric system<sup>[2]</sup>. In recent years harvesting of solar energy has attracted a lot of

attention due to the realization of dye-sensitized solar cells (DSSCs)<sup>[3]</sup>. The decisive use of various sensitizers including quantum dots in the system is found to be one of the key considerations in the fabrication of efficient DSSCs<sup>4</sup> as the efficient transfer of solar energy from the sensitizers to the nanoparticulate film of a wide band gap oxide semiconductor and eventually the charge separation determines the quality of the DSSCs. Extensive studies in order to quantify the efficacy of the energy transfer in various multi-chromophoric systems in proteins, DNA have been reported from our group<sup>[5–6]</sup>. In a recent study, we have explored the ultrafast dynamics of the excitonic energy from a CdSe/ZnS quantum dot to a chemotherapeutic drug merocyanine<sup>[7]</sup> by using Förster Resonance Energy Transfer (FRET). It is also evident from recent literature that FRET serves as a popular signal transduction mechanism to develop biosensing systems and bioassays for proteins, peptides, nucleic acids and small molecules<sup>[8–13]</sup>. Although the use of ZnO nanoparticles (NPs) in DSSCs<sup>[14]</sup> and photolytic agent<sup>[15–16]</sup> are well documented in the literature, the reports on the light harvesting mechanism of the NPs are sparse. Firstly, we report our studies on the ultrafast dynamics of energy transfer from ZnO NPs to a well known biological marker Oxazine 1 (OX1)<sup>[17]</sup>. The cationic OX1 dye is supposed to bind at the surface of the n-type ZnO NPs. Picosecond-resolved FRET studies of the ZnO–OX1 system confirm that the surface states of the NP's contribute to the light-harvesting process.

The promising DSSC is a relatively new class of low-cost solar cells suitable for renewable electricity generation<sup>[18–19]</sup>. It is based on solar light harvesting of a sensitizing dye (SD) attached to a wide-band gap semiconductor. The process of conversion of solar energy to electrical energy in a DSSC involves SD adsorbed on the surface of a wide band gap n-type metal oxide semiconductor NPs (typically TiO<sub>2</sub><sup>[20]</sup>, ZnO<sup>[14, 21]</sup>, SnO<sub>2</sub><sup>[22]</sup>, Nb<sub>2</sub>O<sub>5</sub><sup>[23]</sup> etc). During operation, photons intercepted by the SD molecules create electron-hole pairs that are rapidly separated at the nanoparticle surface, with electrons injected into the semiconductor NPs and holes leaving the opposite side of the device by means of redox species (usually I<sup>-</sup>/I<sub>3</sub><sup>-</sup>) in a electrolyte in liquid<sup>[24]</sup> or solid state<sup>[14]</sup>. State of the art TiO<sub>2</sub> NP-based DSSCs, which primarily absorbs light in the region of 350–700 nm, offer power conversion efficiency of only 11%<sup>[25]</sup>. It has been recognized that the key improvement of the efficiency of DSSC is to increase their spectral absorption range. In a recent study it has been estimated that a DSSC with power conversion efficiency of 15% using I<sup>-</sup>/I<sub>3</sub><sup>-</sup> redox couple must absorb ~80% of the solar spectrum from 350 nm–900 nm<sup>[26]</sup>.

Light absorption in DSSCs is determined by the molar extinction coefficient of the SD, the surface coverage of the dye (dye molecules nm<sup>-2</sup>), and the total surface area of the oxide film<sup>[3]</sup>. The SD has traditionally been made from ruthenium-based complexes (for example, N719 and Z907)<sup>[25, 27]</sup> that have fairly broad absorption spectra (DI  50 nm) but low molar extinction coefficients (5,000–20,000 M<sup>-1</sup> cm<sup>-1</sup>). Organic dyes have

recently been developed with substantially higher molar extinction coefficients ( $50,000$ – $200,000 \text{ M}^{-1} \text{ cm}^{-1}$ ) but have very narrow spectral bandwidths ( $\sim 50 \text{ nm}$ )<sup>[28]</sup>. As a general rule, dyes that absorb strongly do not typically exhibit broad absorption characteristics<sup>[29]</sup>. In an attempt to enhance light absorption and broaden the spectral response, organic DSSCs<sup>[30]</sup>, co-sensitization of the semiconductor NPs (titania) by dyes with complementary absorption spectra, has recently been demonstrated. However, limitations in the number of available sites at the surface of the semiconductor NPs for the co-sensitizing dyes constrains the total light absorbed in the solar cells.

In order to improve the possibility of enhanced light absorption, the use of FRET between covalently linked energy donor molecules to the SD attached on the semiconductor (titania) surface has been demonstrated in a recent literature<sup>[31]</sup>. One of such studies was able to demonstrate high excitation transfer efficiency ( $> 89\%$ ) between attached dye molecules and an improvement in the device external quantum efficiency of  $5$ – $10\%$  between  $400$  and  $500 \text{ nm}$  spectral range. However, the overall power conversion efficiency enhancement of the DSSC was low ( $< 9\%$ ) that was argued to arise due to an increase in the open circuit voltage rather than an increase in the short-circuit photocurrent density. More recently, it has been demonstrated that unattached, highly luminescent chromophores inside liquid electrolyte can absorb high energy photons and efficiently transfer the energy to the anchored near-infrared SD leading to an increase in optical absorption efficiency<sup>[29]</sup>.

Although most of the reported works on DSSC are based on  $\text{TiO}_2$  porous thin films, various structures of  $\text{ZnO}$  are also being used for DSSC fabrication<sup>[14, 32–34]</sup>. The advantages of using  $\text{ZnO}$  over  $\text{TiO}_2$  are its direct band gap ( $3.37 \text{ eV}$ ), higher exciton binding energy ( $60 \text{ meV}$ ) compared to  $\text{TiO}_2$  ( $4 \text{ meV}$ )<sup>[35–36]</sup> and higher electron mobility ( $200 \text{ cm}^2\text{V}^{-1}\text{s}^{-1}$ ) over  $\text{TiO}_2$  ( $30 \text{ cm}^2\text{V}^{-1}\text{s}^{-1}$ )<sup>[37]</sup>. However, the efficiency of the DSSC based on  $\text{ZnO}$  nanostructures is still very low ( $5\%$ )<sup>[38]</sup>. One of the possibilities to enhance the efficiency of  $\text{ZnO}$ -based DSSC is the enhancement of light absorbing ability of the DSSC. It has to be noted that  $\text{ZnO}$  can absorb high energy photons ( $> 3.37 \text{ eV}$ ) and offers photoluminescence (PL) in the visible-region ( $2.25 \text{ eV}$ )<sup>[15]</sup>. Careful use of the defect mediated  $\text{ZnO}$  PL for the excitation of the surface adsorbed SD, in order to enhance the overall efficiency of the  $\text{ZnO}$ -based DSSC, is the motive of the present study. In this article we would describe our studies on the FRET dynamics from a  $\text{ZnO}$  semiconductor nanoparticle surface adsorbed N719 dye used as sensitizer. By using steady state picosecond resolved fluorescence spectroscopy we have demonstrated that PL from a  $\text{ZnO}$  NPs can be used to excite the SD molecule for the enhancement of light absorption possibility. The study also reveals that physical migration of the photo-induced charge from the  $\text{ZnO}$  NPs to the SD molecules is insignificantly small in the de-excitation of the

semiconductor NPs. The effect of ZnO NPs mediated light harvesting process on the overall efficiency of a model DSSC has also been demonstrated.

Quantum dots and metal NPs are of great interest because of their unique electronic, optical, and magnetic properties<sup>[39–43]</sup>. In particular, noble metal NPs having diameters below 10 nm have been the focus of recent works<sup>[44–45]</sup> due in part to their enhanced reactivities. For example, Au NPs of 3 to 8 nm diameter have been shown to tune the catalytic properties of TiO<sub>2</sub><sup>[46–48]</sup>. In the structure of composite nanocluster-based DSSCs, Au NPs are employed to facilitate efficient charge separation, thus serving as a Schottky barrier for reducing the rate of electron-hole recombination<sup>[49]</sup>. Tetsu *et al.*<sup>[50]</sup> studied the enhancement of anodic photocurrents induced by visible light irradiation in a device based on Au NPs deposited on TiO<sub>2</sub> films. Their data indicate that using Au Schottky contacts in photovoltaic cells may yield improved device performance. In an earlier investigation<sup>[51]</sup> by Kamat and co-workers, it was shown that the photoelectro-chemical performance of nanostructured TiO<sub>2</sub> films could be improved by coupling to noble metal NPs. Using the hypothesis of Fermi level equilibration, it has been possible to understand the increase in the photo-voltage of TiO<sub>2</sub>–Au films<sup>[51–52]</sup> as well as the charging effects in metal-semiconductor colloids<sup>[53–56]</sup>. Although there have been many attempts to obtain improved device performance with metal-semiconductor nanocomposites (NCs), the mechanism of charge separation as well as the excitation-dependent interfacial charge transfer kinetics in the nanoscale regime are yet to be fully understood.

The improved performance of photoactive processes and devices has typically been achieved with composite nanostructures based on semiconductor oxides, such as TiO<sub>2</sub> and ZnO, modified with noble metal NPs. A systematic study of the energetics of such NC systems is important for tailoring the properties of next-generation nano-devices. The mediating role of noble metals in storing and shuttling photogenerated electrons from the semiconductor to an acceptor in a photocatalytic process can be understood by designing metal-semiconductor NC structures. Among direct band-gap crystals, ZnO has a wide band gap of 3.37 eV and a large exciton binding energy of 60 meV at room temperature. Two PL bands are usually found: a relatively weak and narrow UV emission band (band-gap emission) around 370 nm (3.35 eV), which is just below the onset of absorption, and a much stronger and broader visible emission band with a maximum near 550 nm (2.25 eV). The UV emission band is due to the radiative annihilation of excitons, the high binding energy of which permits observation even at significantly elevated temperatures<sup>[57]</sup>. The green emission is known to come from the defect centers located near the surface of the NPs<sup>[58]</sup>. Numerous studies have been conducted to improve the band-gap emission by controlling the influence of defect states for the improvement of emission efficiency in semiconductors<sup>[59–60]</sup>. In an earlier study<sup>[61]</sup> with ZnO–Pt NCs,

it was reported that the band-gap emission is enhanced substantially, while the defect emission is suppressed. The underlying mechanism behind enhancement of the band-gap emission and quenching of the defect-mediated green emission is a combination of the energy transfer between defects and surface plasmon (SP) resonance in Pt NPs, as well as electron-hole pair generation and recombination processes in ZnO nanorods. A similar study<sup>[62]</sup> with Au-capped ZnO nanorods indicates that the suppression of the green emission might be due to a combined effect of Au SP and passivation of the ZnO nanorod (NR) surface traps.

Here we describe our investigation on the mechanism of pronounced intrinsic emission from colloidal ZnO and ZnO–Au NCs upon above band-edge and below band-gap excitation. To probe the correlation between dynamics of photo-generated carrier trapping at the defect sites and kinetics of charge migration from ZnO and ZnO–Au semiconductors, methylene blue (MB) degradation was examined using UV light and optical filters. Photostability and luminescence studies from a ZnO–Au NC colloidal dispersion show that FRET dynamics from donor semiconductor to gold acceptor can be observed. Finally, we have designed a model DSSC based on ZnO NPs which leads to an increase in short circuit photo-current ( $J_{sc}$ ) and improved overall efficiency ( $\eta$ ) in the presence of Au NPs. The reason behind the giant improvement in efficiency is also clarified by photoconductivity measurements of the ZnO NP and ZnO–Au NC thin films.

## 2. MATERIALS AND METHODS

### 2.1. Preparation of ZnO and ZnO–Au Nanocolloids

In order to synthesize colloidal solution of ZnO NPs, zinc acetate dihydrate,  $Zn(CH_3COO)_2 \cdot 2H_2O$  (Merck) was used as starting material. ZnO NP colloidal solution in ethanol was synthesized following our earlier reports<sup>[15, 63–64]</sup>. A 20 ml 4 mM zinc acetate solution was prepared in ethanol (Merck) followed by a dilution up to 50% by adding another 20 ml fresh ethanol to the solution. Then 20 ml of 4 mM NaOH solution in ethanol was added to it under constant stirring. The reaction beaker was then kept in a preheated water bath at 60°C for 2 hours to hydrolyze, after which a transparent ZnO NP colloid was obtained.

ZnO–Au NC colloid was prepared by in situ synthesis of Au NPs on the surface of the ZnO NPs. 5 ml of 1 mM chloroauric acid [ $HAuCl_4 \cdot H_2O$ ] (Sigma) ethanolic solution was slowly added to the as synthesized ZnO NP colloid under constant stirring at room temperature. The stirring was continued for 15 minutes. Then 7 ml of 5 mM sodium borohydride,  $NaBH_4$  (Sigma) in ethanol solution was added drop-wise to the solution in order to reduce the gold chloride to Au NPs. Immediately after adding  $NaBH_4$  the solution becomes red from pale yellow color indicating the formation of the Au NPs

in the ZnO NP colloid. The weight ratio between ZnO and Au after the preparation process was found to be 1.3:1. The colloidal solutions of ZnO NPs and ZnO–Au NCs are used to perform all the spectroscopic studies.

## 2.2. Fabrication of ZnO NP-Based DSSCs

The DSSC photoelectrode was prepared by *in-situ* synthesis of ZnO NPs on commercial fluorinated tin oxide (FTO) glass substrate (Asahi, Japan) using a simple hydrothermal process<sup>[65]</sup>. ZnO NPs were synthesized on to the substrate by dropping ethanolic solutions of 1 mM zinc acetate dehydrate followed by annealing at 350°C for 5 hours. The ZnO NP photoelectrode was then soaked in a 0.5 mM ethanolic solution of dye N719 (Solaronix, Switzerland) for 24 hours for the adsorption of dye and rinsed properly with dry ethanol. A platinized FTO glass 8Ω/square (Asahi, Japan) was used as counter electrode. The platinum layer was deposited on the FTO surface by thermal decomposition of platinum chloride, [H<sub>2</sub>PtCl<sub>6</sub>·H<sub>2</sub>O] (Fluka) at 385°C for 15 minutes. The counter electrode was then placed on top of the photoelectrode and a single layer of 50 mm thick surlyn 1720 (Dupont) was used as a spacer between the two electrodes. The DSSC was then sealed properly using the DSSC assembly machine developed in our lab. The liquid electrolyte composed of the 0.5 M LiI  5M I<sub>2</sub> and 0.5 M 4-tert-butyl pyridine (TBP) in acetonitrile (ACN) was then filled in the cell using capillary force through small holes drilled on the counter electrode. Finally, the holes in the counter-electrode were sealed to prevent the electrolyte leaking. I–V characteristic measurements of the DSSCs were performed under AM1.5G sun irradiation (100 mW/cm<sup>2</sup>) using 150W small beam simulator (Sciencetech, model SF150).

## 2.3. Characterization Methods

High resolution TEM experiments are performed in FEI (Technai S–twin) instrument operated at 200 kV. Scanning electron microscopy (SEM) images were taken using a JEOL JSM–6301F operated at 20 kV. Steady-state absorption and emission spectra were measured with a Shimadzu UV–2450 spectrophotometer and Jobin Yvon Fluoromax–3 fluorimeter, respectively. All the photoluminescence transients were taken using the picoseconds-resolved time-correlated single photon counting (TCSPC) technique. We used a commercially available picosecond diode laser-pumped (LifeSpec–ps) time-resolved fluorescence spectrophotometer from Edinburgh Instruments, U.K. The picosecond excitation pulse from the picoquant diode laser was used at 375 nm with instrument response function (IRF) of 80 ps. A microchannel–plate–photomultiplier tube (MCP–PMT, Hammamatsu) was used to detect the photoluminescence from the sample after dispersion through a monochromator. For all transients the polarizer on the emission side was adjusted to be at 55° (Magic angle) with respect to

the polarization axis of the excitation beam. The observed fluorescence transients were fitted by using a nonlinear least square fitting procedure

to a function ( $X(t) = \int_0^t E(t')R(t-t')dt'$ ) comprising of convolution of the IRF

( $E(t)$ ) with a sum of **exponentials** ( $R(t) = A + \sum_{i=1}^N B_i e^{-t/\tau_i}$ ) with pre-

exponential factors ( $B_i$ ), characteristic lifetimes ( $\tau_i$ ) and a background ( $A$ ). Relative concentration in a multi-exponential decay is finally expressed

as,  $c_n = \frac{B_n}{\sum_{i=1}^N B_i} \times 100$ . The average lifetime (amplitude-weighted) of a multi-

exponential decay<sup>[66]</sup> is expressed as  $\tau_{av} = \sum_{i=1}^N c_i \tau_i$

In order to estimate FRET efficiency of the donor (ZnO) and hence to determine distance of donor-acceptor pairs, we followed the methodology described in reference 67. The Förster distance ( $R_0$ ) is given by,

$$R_0 = 0.211 \times [\kappa^2 n^{-4} Q_D J]^{1/6} \quad (\text{in } \text{\AA}) \quad (1)$$

where,  $\kappa^2$  is a factor describing the relative orientation in space of the transition dipoles of the donor and acceptor. For donor and acceptors that randomize by rotational diffusion prior to energy transfer, the magnitude of  $\kappa^2$  is assumed to be 2/3. The refractive index ( $n$ ) of the medium is assumed to be 1.4.  $Q_D$ , the integrated quantum yield of the donor in the absence of acceptor is measured to be  $3.8 \times 10^{-3}$ .  $J$ , the overlap integral, which expresses the degree of spectral overlap between the donor emission and the acceptor absorption, is given by,

$$J = \frac{\int_0^{\infty} F_D(\lambda) \epsilon_A(\lambda) \lambda^4 d\lambda}{\int_0^{\infty} F_D(\lambda) d\lambda} \quad (2)$$

where,  $F_D(\lambda)$  is the fluorescence intensity of the donor in the wavelength range of  $\lambda$  to  $\lambda+d\lambda$  and is dimensionless;  $\epsilon_A(\lambda)$  is the extinction coefficient (in  $M^{-1} \text{ cm}^{-1}$ ) of the acceptor at  $\lambda$ . If  $\lambda$  is in nm, then  $J$  is in units of  $M^{-1} \text{ cm}^{-1} \text{ nm}^4$ . The estimated value of the overlap integral is  $3.79 \times 10^{15}$ . Once the value of  $R_0$  is known, the donor-acceptor distance ( $r_{DA}$ ) can be easily calculated using the formula,

$$r_{DA}^6 = \frac{[R_0^6(1-E)]}{E} \quad (3)$$

Here  $E$  is the efficiency of energy transfer. The transfer efficiency is measured using the relative fluorescence lifetime of the donor, in absence ( $\tau_D$ ) and presence ( $\tau_{DA}$ ) of the acceptor.

$$E = 1 - \frac{\tau_{DA}}{\tau_D} \quad (4)$$

We are also interested to obtain the thickness of the surface layer emitting visible light by using a simple model<sup>[67]</sup>. In order to obtain the below band gap (BBG) (550 nm, *i.e.* 2.25 eV) and near band edge (NBE) (365 nm, *i.e.* 3.39 eV) emission of the ZnO NPs, we have excited the sample with 320 nm (3.87 eV) light. The luminescence peak intensity ratio of the NBE to BBG emission for spherical particles of radius  $r$  and with a surface recombination layer of thickness  $t$ , is given by,<sup>[68]</sup>

$$\frac{I_{NBE}}{I_{BBG}} = C \left( \frac{r^3}{3rt(r-t) + t^3} - 1 \right) \quad (5)$$

The constant  $C$ , along with other quantities, contains the oscillator strengths which in turn depend on the particle morphology. In order to calculate  $t$  from the above equation we have taken the magnitude of  $C$  as 3.89 for small spherical particles<sup>[68]</sup> with radius  $r \approx 3$  nm. In our system  $I_{NBE}(365\text{nm})/I_{BBG}(550\text{nm}) \approx 0.853$ . Putting the values in Equation 5, the thickness of the surface layer,  $t$ , was found to be 1.30 nm. It represents an effective distance from the surface (effective diffusion length), within which the excited carriers recombine at the surface.

We have studied the complexation between ZnO NP with different concentrations of N719 dye. The ratio of the fluorescence intensity of the ZnO NP in absence ( $I_0$ ) and presence ( $I$ ) of the quencher N719 was plotted in Figure 5c and 5d using Stern-Volmer equation<sup>[66]</sup>.

$$\frac{I_0}{I} \text{ or } \frac{\tau_0}{\tau} = 1 + K_{SV}[Q] \quad (6)$$

where,  $\frac{I_0}{I}$  is the relative steady state emission intensity,  $\frac{\tau_0}{\tau}$  is the relative excited state lifetime and  $K_{SV}$  is Stern–Volmer constant.

In order to measure the device performance, the incident photon-to-current conversion efficiency (IPCE) and photocurrent–voltage (J–V)

characteristics were determined. The IPCE, defined as the number of electrons collected per incident photon, was evaluated from short-circuit photocurrent ( $J_{sc}$ ) measurements at different wavelengths ( $\lambda$ ), and the IPCE was calculated using Equation 7,

$$IPCE\% = \left[ 1240 \times J_{sc} \left( A / cm^2 \right) \right] / \left[ \lambda (nm) \times P \left( W / cm^2 \right) \right] \times 100\% \quad (7)$$

where, P is the incident light power. The fill factor (FF) and power conversion efficiency ( $\eta$ ) of the solar cells can be determined from Equations 8 and 9,

$$FF = V_M J_M / V_{OC} J_{SC} \quad (8)$$

$$\eta = V_{OC} J_{SC} / FF \quad (9)$$

where,  $V_M$  and  $J_M$  are the voltage and current density at the maximum power output,  $J_{SC}$  and  $V_{OC}$  are the short-circuit current and open-circuit voltage, respectively<sup>[69-70]</sup>.

### 3. RESULTS AND DISCUSSION

#### 3.1. Dynamics of Light Harvesting in ZnO Nanoparticles<sup>[71]</sup>

The absorption and emission spectra of ZnO (energy donor) and Oxazine 1 (energy acceptor) are shown in Figure 1. It is clearly evident from the broad emission peak of the ZnO NPs in ethanol at 550 nm that the photoluminescence is essentially dominated by the excitonic transition at the surface of the ZnO NPs and defect mediated origin of the green luminescence<sup>[68,72]</sup>. A. van Dijken *et al.*<sup>[73]</sup> proposed that the visible emission is due to the recombination of an electron from the conduction band with a deep electron trapping centre of  $V_O^{++}$ , which is considered as oxygen vacancy center. Alternatively, K. Vanheusden *et al.*<sup>[74]</sup> suggested that the recombination of isolated  $V_O^+$  center with photoexcited holes are responsible for the green emission. Because of the large surface-to-volume ratio of our ZnO NPs, efficient and fast trapping of photogenerated holes at surface sites can be expected. However, the broad emission band can be decomposed into two components. The predominant emission energy is concentrated around the  $\lambda = 550$  nm (2.25 eV) line while a smaller emission band occurs at around  $\lambda = 495$  nm (2.50 eV). It has been reported that the emission centre around 550 nm occurs from defect states near the surface layer (within a shell of  $t$ ) while the shorter wavelength 495 nm emission occurs from defects near the bulk of the NPs<sup>[67-68]</sup>, which is located inside at a distance  $> t$  from the surface. As the size of the NP is increased, the relative contribution of the 495 nm emission increases. The absorption and emission spectra of the acceptor OX1 at the surface are also consistent with that reported in the literature<sup>[17]</sup>. The consistency of the spectral pattern of the

acceptor OX1 with the other studies clearly rules out the possibility of any damage of the OX1 molecule at the ZnO surface. The spectral overlap of the ZnO emission spectrum with that of the OX1 absorption spectrum is shown in Figure 2a. The faster excited state lifetime of the ZnO–OX1 adduct with respect to that of the free ZnO NPs is clearly noticeable from Figure 2b. The baseline upliftment comes from the long lifetime component which is not ending in our experimental time window.

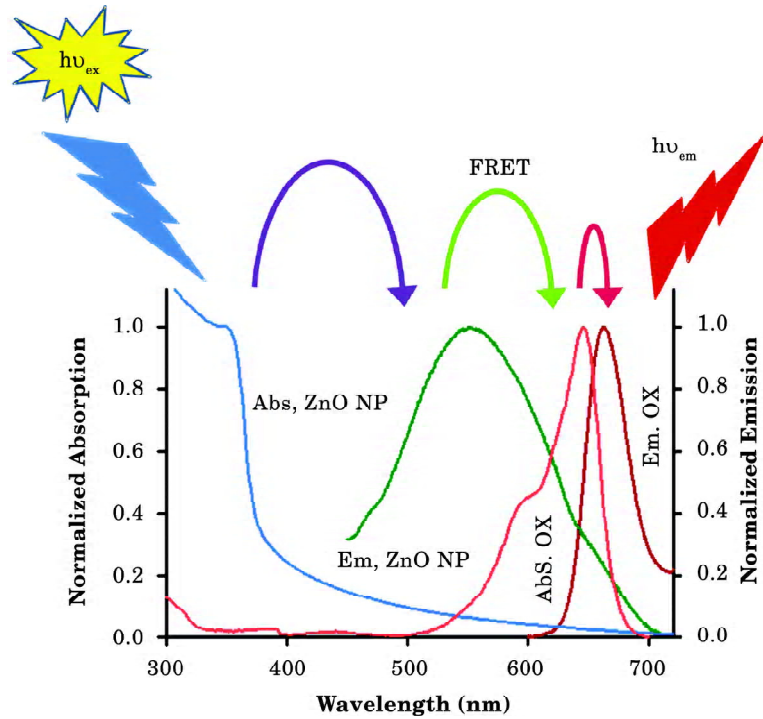


**Fig. 1:** Normalized absorption (blue) and emission (green) spectra of ZnO NP with diameter of ~6 nm. Cascade harvesting of blue photon to red photon in the ZnO NP–OX1 complex is shown. The normalized absorption and emission of OX1 are shown.

The detailed spectroscopic and fitting parameters of the fluorescence decays are tabulated in Table 1. From the average lifetime calculation for the ZnO–OX1 complex, we obtain the effective distance between the donor and the acceptor,  $r_{DA} \approx 1.58$  nm, using Equation 3 and 4. It is noted that  $r_{DA}$  is much smaller than the radius of the NP (~3 nm; inset Figure 2b) and is comparable to the thickness  $t$  of the surface layer of the NPs *i.e.*,  $r > r_{DA} \approx t$ . In the case of organic acceptor molecules at the surface of a semiconductor (CdSe) quantum dot donor, the overall donor-acceptor distance is reported to be nearly equal (or larger) to the radius of the donor quantum dot<sup>[7]</sup>. The relatively shorter donor-acceptor distance in the case of ZnO–OX1 system compared to other systems<sup>[7]</sup> can be rationalized from the fact that the

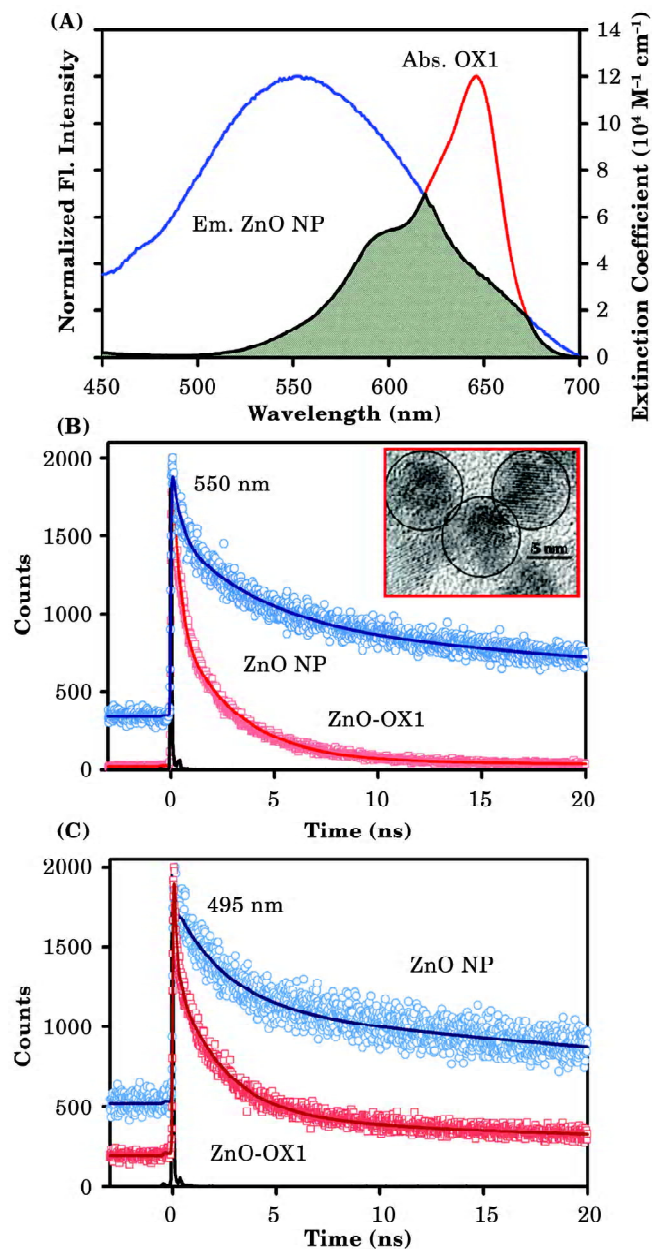


**Fig. 2:** (a) Steady state absorption spectra of OX1 (red) and emission spectra of ZnO NP (blue) are shown. An overlapping zone between emission of ZnO NP and absorption of acceptor OX1 is indicated as a green shaded zone. The picosecond-resolved fluorescence transients of ZnO NP, in absence (blue) and in presence of acceptor OX1 (red) (excitation at 375 nm) collected at (b) 550nm and (c) 495 nm, are shown. Inset of the Figure 2(b) shows the high resolution transmission electron microscope (HRTEM) image of ZnO NPs.

origin of the PL peaking at 550 nm is essentially from the surface layer of approximate thickness 1.3 nm of the ZnO NPs.

In order to compare the FRET from other emission centres (Scheme 1) of ZnO NPs, we have also studied the energy transfer dynamics at  $\lambda_{em} = 495$  nm. The relative dynamical quenching of the ZnO–OX1 system with respect to free ZnO at 495 nm is shown in Figure 2c. The relevant data are also given in Table 1. From the average lifetime data and using equation 3 and 4 we obtain for the 495 nm emission  $r_{DA} = 2.25$  nm, which is much larger than that observed at 550 nm. In this case  $r \approx r_{DA} > t$  clearly indicating that the emission at 495 is from defect sites located within the bulk of the NPs. The efficiency of the FRET (E) as obtained from Equation 4 is highest for the 550 nm line (93%) and much smaller (63%) for the 495 nm line.

**Table 1:** Picosecond-resolved luminescence transients of various samples. The emission from ZnO NPs (emission at 495 nm and 550 nm) was detected with 375 nm excitation. The emission of the acceptor OX1 in ethanol and at ZnO surface (emission at 665 nm) was detected with 633 nm laser excitation. Numbers in the parenthesis indicate relative weightage.

Sample	$\tau_1$ (ns)	$\tau_2$ (ns)	$\tau_3$ (ns)	$\tau_{av}$ (ns)
ZnO–NP (550nm)	47.583±0.75 (40%)	3.787±0.19 (23%)	0.281±0.003 (37%)	20.32
ZnO NP–OX1 (550nm)	19.044±0.73 (1.4%)	2.797±0.02 (33.3%)	0.259±0.005 (65.3%)	1.37
ZnO NP (495nm)	35.05±0.87 (30%)	2.48±0.15 (30%)	0.089±0.009 (40%)	11.29
ZnO NP–OX1 (495nm)	32.530±0.39 (10%)	2.320±0.02 (36%)	0.148±0.006 (54%)	4.17
ZnO nanorod (550nm)	10.372±0.09 (6.3%)	2.440±0.02 (28.2%)	0.159±0.004 (65.5%)	1.45
ZnO rod–OX1 (550nm)	8.454±0.06 (5.1%)	1.515±0.01 (21.0%)	0.087±0.003 (73.9%)	0.82
OX1 in EtOH (665 nm)	0.693±0.001 (100%)	–	–	0.693
ZnO NP–OX1 (665 nm)	0.867±0.002 (100%)	–	–	0.867

We have extended our studies on the attachment of the OX1 molecules at the surface of the ZnO nanorods (NRs). NRs are very important components for the state of the art ZnO–based DSSCs<sup>[75]</sup>. The morphology of ZnO NR was characterized by scanning electron microscopy (SEM). A typical SEM image of ZnO NR (Figure 3b inset) shows 400 nm long and 40 nm wide NR growths. The NRs are found to offer photoluminescence peaking at 495 nm. The spectral characteristic is consistent with the fact that the emission is dominated by the bulk state of the semiconductor<sup>[68, 76]</sup>. As shown in Figure 3b, the fluorescence quenching of the ZnO NR–OX1 adduct offers insignificantly small quenching with efficiency 44% compared to that of the free NRs in the bulk ethanol. No attempt has been made to estimate

donor-acceptor distance in the case of NR–OX1 adduct because of the inadequate quantum yield of the ZnO NRs.

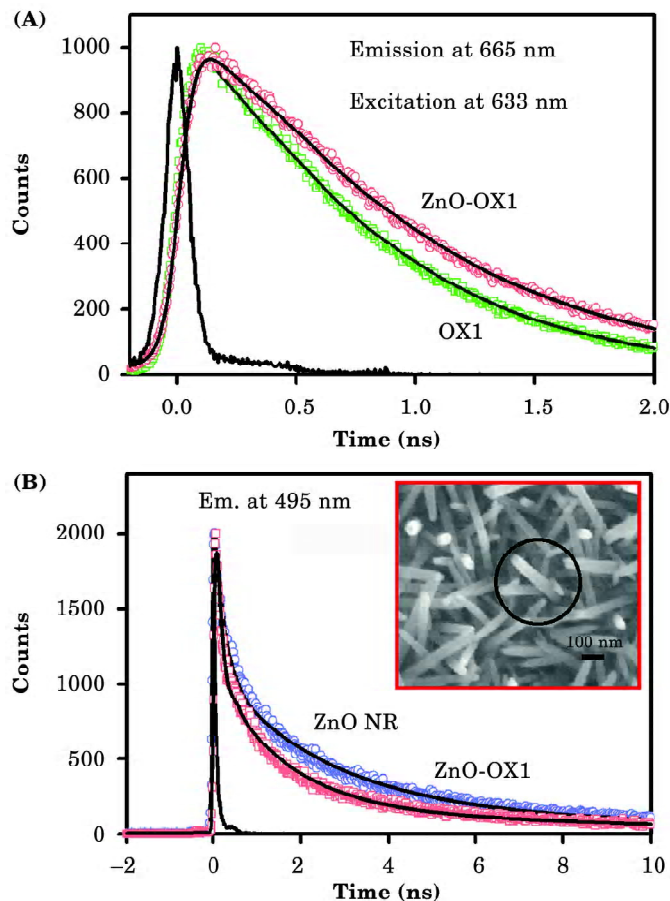
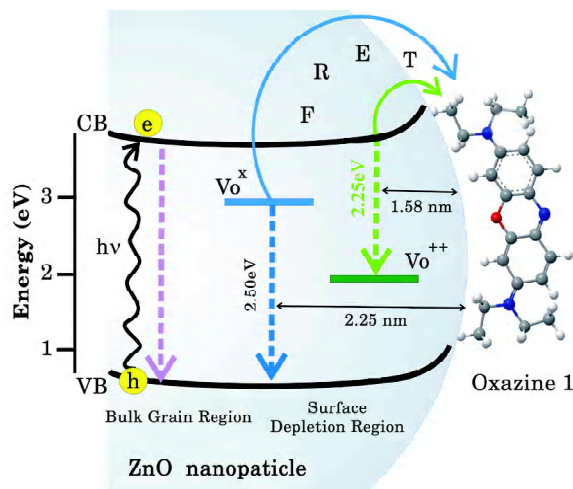


**Fig. 3:** (a) The picoseconds-resolved fluorescence transients of acceptor OX1 (green) and OX1 in presence of ZnO NP (red), (excitation at 633 nm) collected at 665 nm, (b) Time resolved quenching spectrum of ZnO nanorod in presence (red) and absence (blue) of OX1 (excitation at 375 nm) collected at 495 nm. Inset of the figure shows the Scanning Electron Microscope (SEM) image of ZnO nanorod.

Our experiments also explore the possibility of charge transfer from the ZnO surface. The acceptor molecule OX1, is well known to be a potential electron acceptor<sup>[17]</sup>. It has been demonstrated that the molecule offers an ultrafast fluorescence decay following an electron transfer reaction<sup>[77]</sup>. However, from Figure 3a it is evident that the fluorescence decay of OX1 at the ZnO surface is slightly longer than that in the bulk ethanol. The observation clearly rules out the possibility of any kind of electron transfer reaction in the quenching process of the ZnO NPs. On the other hand slight

lengthening of the excited state lifetime of the acceptor molecule OX1 confirms its adsorption at the ZnO surface, which makes OX1 molecule more restricted.



**Scheme 1:** Schematic diagram of ZnO NPs–OX1 nanocomposite depicting the FRET dynamics from different oxygen vacancy centres ( $V_o^{++}$ ,  $V_o^x$ ) of ZnO NPs to OX1 molecules. Singly charged oxygen vacancy centre ( $V_o^+$ ), present in the surface depletion region, captures a hole to generate  $V_o^{++}$  centre, leading to an emission in with a peak in the vicinity of 2.25 eV (550 nm). In absence of depletion region  $V_o^+$  becomes neutral centre ( $V_o^x$ ) by capturing one electron from the conduction band which is responsible for an emission at 2.50 eV (495 nm). Typical FRET distances from different energy states of ZnO NPs to surface adsorbed OX1 are also shown. The band gap excitation (3.87 eV, i.e 320 nm) is shown by curved arrows.

### 3.2. Role of Resonance Energy Transfer in Light Harvesting of Zinc Oxide based Dye Sensitized Solar Cells<sup>[78]</sup>

The HRTEM image of the ZnO NPs is shown in Figure 4a. Predominance of NPs with diameters of 6–7 nm were found in the synthesized colloids (inset of Figure 4a). Figure 4b shows the UV–vis absorption spectra of ZnO NP and dye N719. The PL spectrum of the ZnO NPs upon excitation with 375 nm is also shown in the figure. Significant spectral overlap of the ZnO PL spectrum with that of the absorption of the N719, which justifies the possibility of energy transfer from ZnO to the N719 SD molecules, is clearly evident from the figure. In order to investigate the complexation of ZnO NPs with the SD N719, we have studied the steady-state PL of the ZnO NPs in the presence of various concentrations of N719 as shown in Figure 5a. We have also studied the PL transient at 550 nm (excitation at 375 nm) (Table 2). The transients in the absence and presence of various N719 concentrations are shown in Figure 5b. The PL quenching as evident from the steady-state and time-resolved PL studies shows the affinity of the

N719 dyes with the ZnO-NPs. Detailed Stern-Volmer (S-V) analysis on the quenching of the ZnO PL (as shown in Figures 5a and 5c) reveals the S-V constants to be  $K_{SV}(\text{steady state}) = 1.14 \times 10^7 \text{ M}^{-1}\text{S}^{-1}$  and  $K_{SV}(\text{time resolved}) = 0.87 \times 10^7 \text{ M}^{-1}\text{S}^{-1}$ , respectively. The similarity of  $K_{SV}$  constants from steady-state and time-resolved measurements indicate the ZnO PL quenching to be dynamic in nature. In other words, the possibility of formation of non-fluorescent ZnO-SD complex in the ground state is found to be negligibly small.

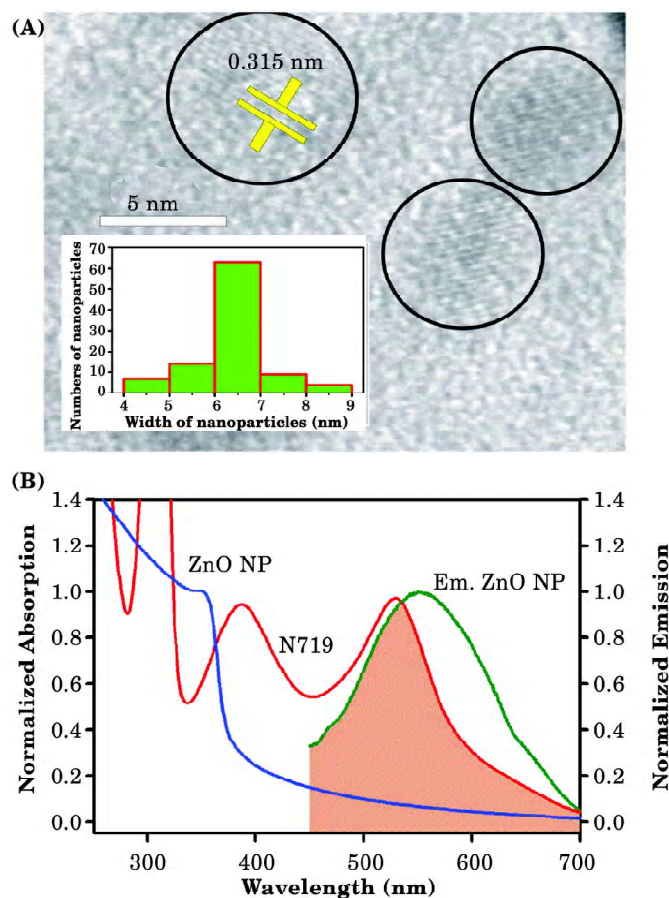


**Fig. 4:** (a) High resolution transmission electron micrograph (HRTEM) showing the ZnO NPs with ~3 nm radius. Inset shows the size distribution of the ZnO NPs. (b) Steady state absorption spectra of ZnO NP (red), N719 and emission spectra of ZnO NP (blue) are shown. An overlapping zone between emission of ZnO NP and absorption of acceptor N719 is indicated as a red shaded zone.

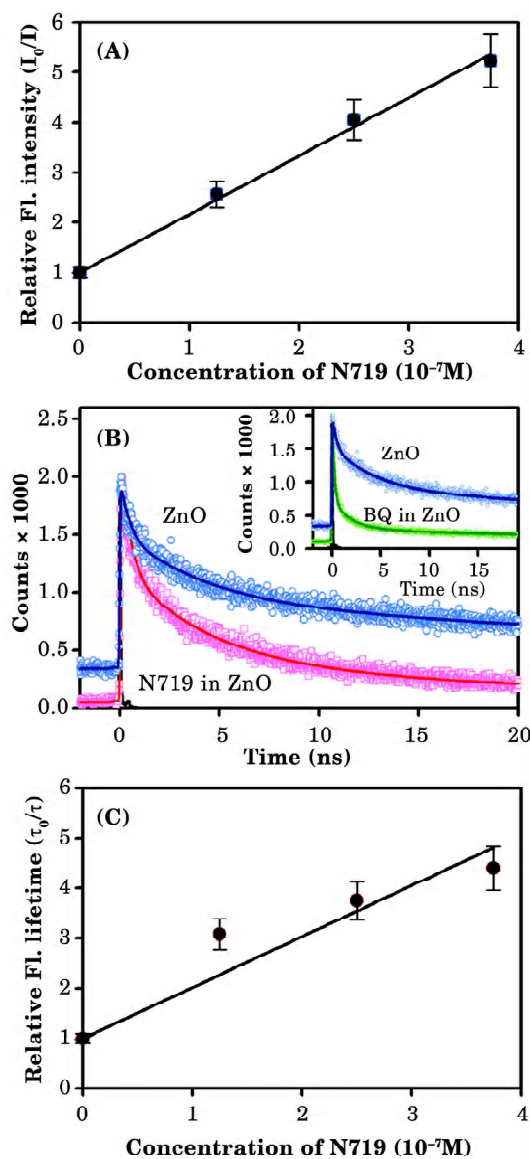


**Fig. 5:** (a) Steady-state emission intensity of ZnO NPs (excitation at 375nm) in presence of increasing concentration of N719 dye relative to that of ZnO emission without N719. (b) The picosecond-resolved fluorescence transients of ZnO NP, in absence (blue) and in presence of acceptor N719 (red) (excitation at 375 nm) collected at 550 nm. Inset shows the faster PL decay of ZnO-NP in presence BQ. (c) Excited state lifetime of the PL emission of ZnO NPs (excitation at 375nm) in presence of increasing concentration of N719 dye relative to that of ZnO emission without N719 is shown.

**Table 2:** Picosecond-resolved luminescence transients of ZnO NPs in the presence and absence of N719. The emission from ZnO NPs (emission at 550 nm) was detected with 375 nm excitation laser excitation. Numbers in the parenthesis indicate relative weightage.

<i>Sample</i>	$\tau_1$	$\tau_2$	$\tau_3$	$\tau_{avg}$
<b>ZnO NP (bare)</b>	47.58ns (41%)	3.78ns (23%)	0.280ns (36%)	20.32 ns
<b>ZnO NP + N719 dye</b>	29.12ns (12%)	3.86ns (38%)	0.344ns (50%)	5.25 ns
<b>ZnO NP + BQ</b>	30.20ns (6%)	1.93ns (18%)	0.187ns (76%)	2.20 ns

<sup>a</sup>The emission from ZnO NPs (emission at 550 nm) was detected with 375 nm excitation laser excitation. Numbers in the parentheses indicate relative weightage.

The dynamic nature of the PL quenching of ZnO NPs upon complexation with N719 is further justified from the FRET of the PL to the surface adsorbed SD N719. The overall FRET efficiency is found to be 74%. In this case the spectral overlap integral,  $J$  (Equation 2) and the Förster distance ( $R_0$ ) are found to be  $6.597 \times 10^{14}$  and 1.84 nm, respectively. From FRET dynamics, it has to be noted that the effective distance ( $r_{DA}$ ) between the donor (ZnO NP) and the acceptor (N719) is 1.54 nm which is much lower than that of the average radii of the NPs ( $\sim 3$  nm). In a FRET study<sup>[5]</sup> on cadmium selenide (CdSe) quantum dot (donor) and a surface adsorbed organic dye (ethidium bromide; acceptor), the donor acceptor distance was found to be close to the radius of the quantum dot. The relatively shorter donor-acceptor distance compared to the radius of the ZnO nanocrystallites in the present study, can be rationalized from the fact that the origin of the PL peaking at 550 nm essentially arises from the crystallites exposed in the surface of the ZnO NPs. It is important to note that the thickness of the surface layer ( $t$ ) obtained from calculation (using Equation 5) is found to be 1.30 nm, which is comparable to the effective distance between the donor and acceptor calculated from FRET study. The observation is consistent with the fact that there is a surface region from where the defect related emission occurs.

In order to investigate the effect of light harvesting of high energy photons by the host ZnO semiconductor in a model DSSC, we have studied the photocurrent-voltage ( $J-V$ ) characteristics as shown in Figure 6a. The  $J-V$  characteristics of the solar cells were measured in two different experimental conditions. Firstly, we have excited the cell with whole solar spectrum (circle-line presentation in Figure 6). In the second case we used a yellow filter to block the solar spectra below 400 nm (high energy photons) as shown in a square-line presentation in Figure 6a. The total light power in both the cases was very carefully maintained at  $100 \text{ mW/cm}^2$ . The open circuit voltage ( $V_{oc}$ ) and short circuit current ( $J_{sc}$ ) increased in the DSSCs, which is excited with UV radiation (without filter). Upon use of the optical filter, a sharp decrease in current from  $1190 \text{ mA/cm}^2$  to  $668 \text{ mA/cm}^2$  was observed. In retrospect, compared to  $43.86 \pm 8 \%$  change in the short

circuit current,  $V_{oc}$  reduced marginally by  $6.66 \pm 4 \%$  while fill factor (FF) reduced only by around  $11.80 \pm 3 \%$  (Table 3). As shown in Figure 4b the SD N719 absorbs very little in the UV region (below 400 nm) of the solar spectrum. Thus it is expected that the efficiency of the solar cell will not be affected much on the presence of high energy photons due to the absence of noticeable optical absorption in the dye at lower wavelengths (below 400 nm). This observation clearly demonstrates that ZnO DSSCs can harvest high energy photons as well. High energy photons were found to have a minimum effect on the solar cell performance of  $TiO_2$  based solar cell with same SD (Figure 6b). From these observations (Figure 6) and also Table 3, we can see that the efficiency of ZnO-based DSSC increases by  $54.15 \pm 10 \%$  if the UV portion of the AM1.5 spectra is employed as well compared to a marginal  $8.29 \pm 4 \%$  increase in efficiency in the case of  $TiO_2$ -based DSSCs. It is clear that harvesting of high energy photons in the case of  $TiO_2$ -based DSSCs does not contribute appreciably to the enhancement of the device

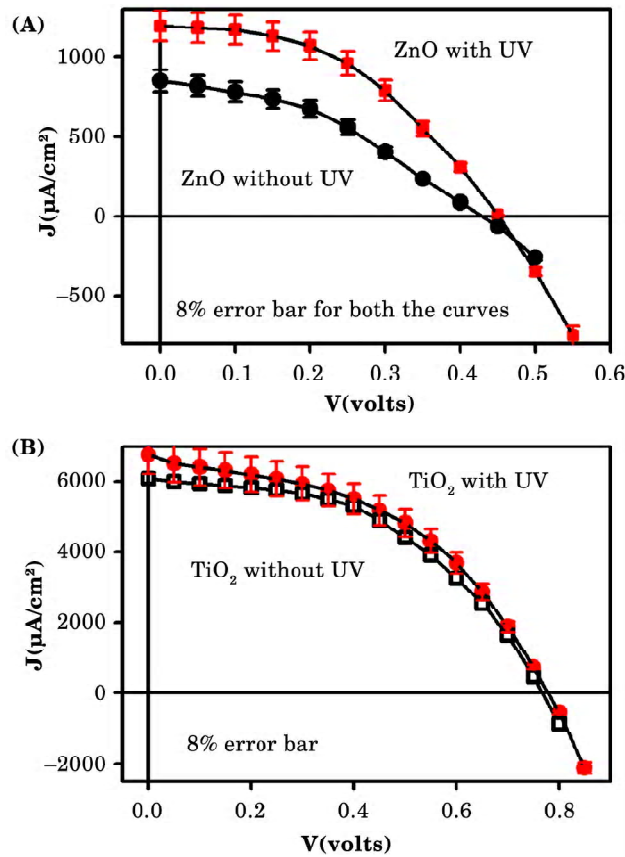


**Fig. 6:** (a) I–V curves of (a) ZnO NP (b)  $TiO_2$  NP based DSSC in presence and absence of UV.

efficiency. It is worth noting that the efficiency obtained from the model DSSC using NPs is lower compared to the maximum efficiency reported where nanorod has been taken in order to provide higher surface area and better charge transport.

**Table 3:** Device performance<sup>[a]</sup> of the DSSCs with ZnO and TiO<sub>2</sub> NPs.

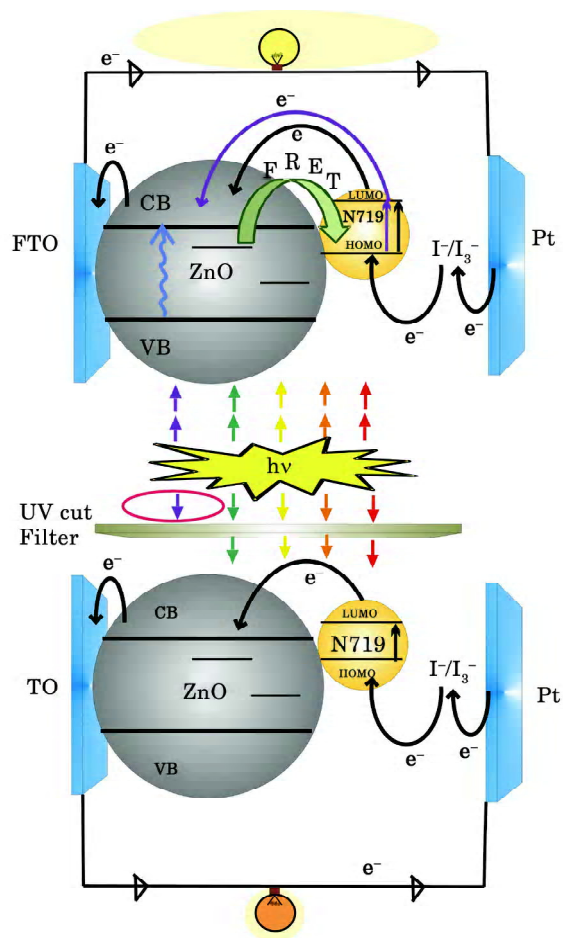
<i>Device with N719</i>	$V_{oc}$ (V)	$J_{sc}$ ( $\mu A/cm^2$ )	FF (%)	$\eta$ (%)
<b>ZnO-NP (with UV)</b>	0.45	1190.00	44.66	0.24
<b>ZnO-NP (without UV)</b>	0.42	668.00	39.39	0.11
<b>TiO<sub>2</sub>-NP (with UV)</b>	0.77	6760.00	46.30	2.41
<b>TiO<sub>2</sub>-NP (without UV)</b>	0.77	6086.67	47.15	2.21

<sup>a</sup>short circuit photocurrent densities ( $J_{sc}$ ), open-circuit voltage ( $V_{oc}$ ), fill factor (FF) and efficiency ( $\eta$ ) (See Equation 8–9)

It has to be noted that N719 is a redox active organic dye<sup>[21]</sup>. In this regard the PL quenching of the ZnO NPs upon adsorption of the dye may be associated with excited state electron transfer from ZnO to the N719 dye molecule. In order to investigate the electron transfer dynamics from the ZnO NPs upon excitation, we have studied the complexation of the NPs with an organic molecule, benzoquinone (BQ) which is well known as an electron acceptor<sup>[79]</sup> and efficiently accepts excited electrons from the surface of semiconductor quantum dots<sup>[80]</sup>.

From our studies the quenching of the PL intensity of ZnO NPs upon complexation with BQ is evident (data not shown). As shown in the inset of Figure 5b, a very sharp decay in fluorescence at 550 nm in the presence of the electron acceptor is indicative of the fast transfer of excited electrons from the conduction band of the ZnO NPs into the LUMO of BQ molecules. The ZnO–BQ system exhibited a faster initial decay with a time period of 0.187 ns with a majority (76%) of the excited electrons following this path (Table 2). The faster decay in presence of BQ as compared to N719 at the same excitation of 375 nm may be indicative of energy transfer from the ZnO donor NPs to the N719 acceptor molecules rather than transfer of electrons. In the case of pure ZnO in ethanol (Figure 5b), the excited state lifetime ( $k_{nr} = 0$ ) of ZnO NPs is 20.32 ns, which yields a radiative rate constant of  $4.92 \times 10^7$ . Upon the addition of N719 and BQ in separate ZnO NP solution, the average lifetimes were found to reduce to 5.25 ns and 2.20 ns, with rate constants of  $1.90 \times 10^8$  and  $4.55 \times 10^8 \text{ M}^{-1}\text{s}^{-1}$ , respectively. We have calculated electron transfer rate, which is directly reflected in the nonradiative rate constants ( $k_{nr}$ ). The calculated  $K_{nr}$  values were found to be  $1.41 \times 10^8$  and  $4.06 \times 10^8 \text{ M}^{-1}\text{s}^{-1}$  for the ZnO–N719 and ZnO–BQ systems, respectively. From the above  $k_{nr}$  values, we can conclude that the electron transfer rate, in case of ZnO–BQ composite, is 3-fold higher compared to the energy transfer in ZnO–N719 system. In the case of electron transfer from excited state ZnO NPs to N719, the short-circuit current of the ZnO NP-based DSSC is expected to be reduced. However, as shown in Figure 6,

the efficiency of the DSSCs in the presence of UV light (i.e. when the ZnO NPs were excited) is increased. Charge conservation clearly rules out any possibility of back electron transfer from ZnO NPs to the SD N719. The overall picture that is evident from our studies is represented in Scheme 2.



**Scheme 2:** It represents a model DSSC based on the ZnO NPs which contains sufficient defect states, namely oxygen vacancy centres near surface depletion region. The system consists of a fluorinated tin oxide (FTO) on which semiconductor ZnO nanoparticle (gray big circle) is fabricated. The sensitizer dye N719 (small yellow circle) is bound to ZnO NP by surface adsorption. The entire structure is immersed in a liquid redox electrolyte ( $I^-/I_3^-$ ). In regular DSSC, light is directly absorbed by the SD, exciting an electron from HOMO to LUMO level. In the proposed configuration which contains a semiconductor having appreciable amount of defect states, an additional “indirect excitation” of N719 is introduced by using the sensitivity of FRET. In the FRET based cell, the semiconductor NP is found to be excited in presence of UV light, by which, an electron is promoted from the valance band to the conduction band,

*Contd... (Scheme 2)*

Contd.(Scheme 2)

followed by energy transfer from excited states of semiconductor to SD N719 *via* FRET. Thereafter, charge separation occurs exactly as it does in regular DSSC and electron is injected from the excited state of the dye into the conduction band of the semiconductor electrode and the electron is thus transported to the charge collector. In presence of a UV cut filter the FRET based cell performs like a regular DSSC as no energy transfer from ZnO NP to SD takes place due to the absence of UV light.

### 3.3. Photoselective Excited State Dynamics in ZnO–Au Nanocomposites and their Implications in Photocatalysis and Dye-Sensitized Solar Cells<sup>81</sup>

The structure, crystalline phase, size, and morphology of ZnO NPs and ZnO–Au NCs were determined (with TEM). Representative high-resolution TEM (HRTEM) images of the ZnO–Au NCs are illustrated in Figure 7a, where the measured average diameters are 6 and 8 nm for ZnO and Au NPs, respectively. From TEM observation it was found that, the ZnO–Au

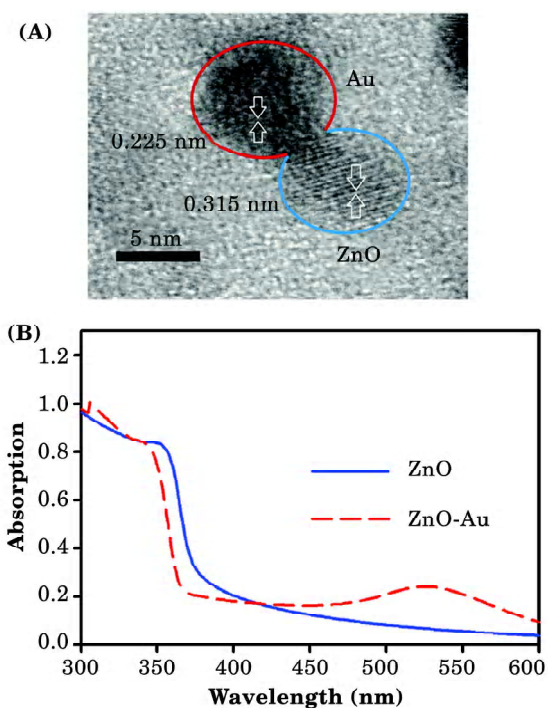


**Fig. 7:** (a) High-resolution TEM (HRTEM) image of dumbbell-like ZnO–Au NCs with Au attached to the ZnO surface. (b) Steady state absorption spectra of bare ZnO NPs (blue) and ZnO–Au NCs (red) showing the SP band at 520 nm.

NCs are fairly monodisperse and their shapes are different from that of the spherical ZnO NPs due to the incorporation of Au components. The higher contrast of Au observed in the TEM image is due to the higher electron density of metallic Au compared to semiconducting ZnO. The relevant TEM images are shown in Figure 8a–c. After the synthesis of ZnO–Au NCs, the Zn:Au weight ratio was calculated by using a field emission–type scanning electron microscope (FEI–SEM; Quanta 200). From EDAX analysis it was found to be 1.3:1 as shown in the table (Figure 8).

The visible absorption spectrum of gold grown onto the ZnO NPs was clearly characterized by the plasmon resonance peak of Au NPs. Figure 7b shows the absorption spectra of the ZnO–Au NCs and pure ZnO NPs. It is

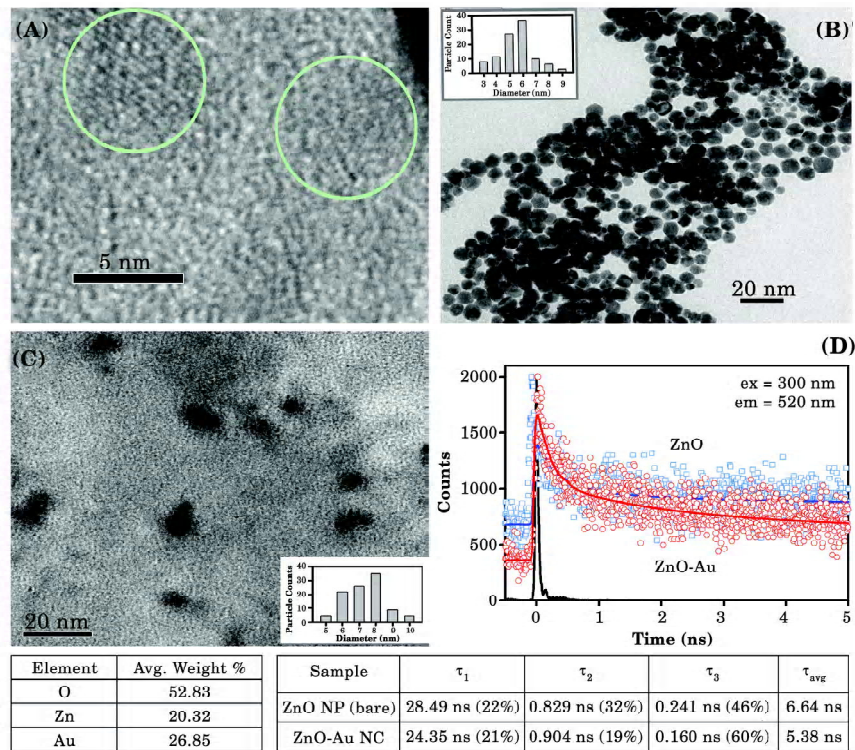


**Fig. 8:** (a) High-resolution TEM (HRTEM) image of bare ZnO NPs. (b) Low-resolution TEM (LRTEM) image of bare ZnO NPs (inset shows particle size distribution of ZnO NPs). (c) Low-Resolution TEM (LRTEM) image of ZnO–Au NCs (inset shows particle size distribution of Au NPs attached to ZnO NPs). Table (left) shows EDAX analysis of ZnO–Au NCs by using a field emission–type scanning electron microscope. Table (right) shows picosecond–resolved luminescence transients of ZnO NPs in the presence and absence of Au NPs. The emissions from ZnO NPs and ZnO–Au NCs (probing at 520 nm) were detected with a 300 nm laser excitation and the numbers in the parentheses indicate relative weightage.

generally believed that the band-edge absorption of semiconductor in the quantum-confined size regime ( $\leq 7$  nm) is dependent on the particle size<sup>[82]</sup>. There is no distinct variation in absorption characteristics in the range 300-420 nm, which implies that no apparent growth of ZnO NPs occurred during the formation of Au on ZnO NPs. An SP band, resulting from Au in the ZnO-Au NCs, centered at  $\sim 525$  nm can also be observed in the NC (Figure 7b). In Figure 9a we have plotted the excitation spectra of bare ZnO NPs and ZnO-Au NCs monitored at the emission peaks (368 nm and 550 nm, respectively). The room temperature PL spectra of both the bare ZnO NPs and ZnO-Au NCs (Figure 9b) are comprised of one broad emission band upon excitation below the band-gap ( $\lambda_{\text{ex}} = 375$  nm) and two emission bands upon excitation above the band-edge ( $\lambda_{\text{ex}} = 320$  nm). The narrow UV band centered at 368 nm is due to exciton recombination. Analysis of the broad emission observed in our sample in the blue-green region shows that it is composed of two emission bands (shown as dotted lines in Figure 9b

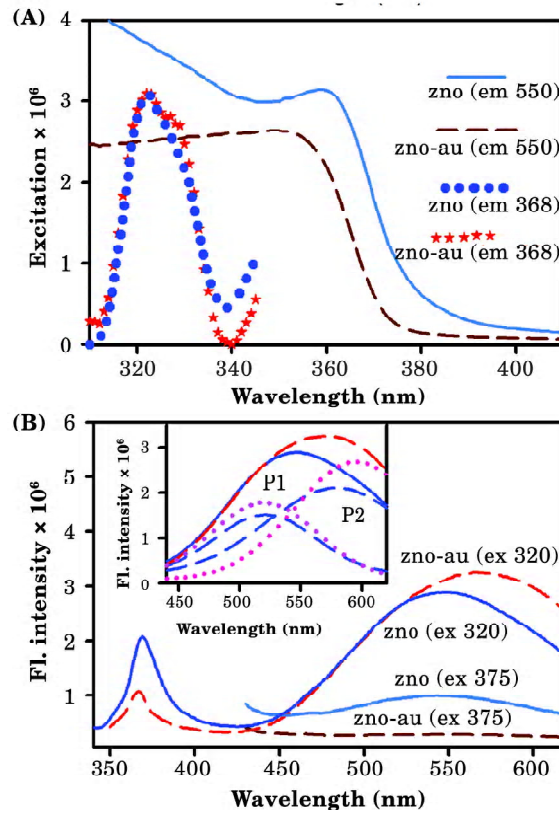


**Fig. 9:** (a) Excitation spectra of ZnO NPs (blue) and ZnO-Au NCs (red) monitored at 368 nm and 550 nm (excitation at 320 and 375 nm, respectively). (b) Steady state emission spectra of ZnO NPs (blue) and ZnO-Au NCs (red) are shown (excitation at 320 and 375 nm). The inset shows that the defect related green emission is composed of two bands, P1 and P2 (see text).



(inset)) which are marked as P1 and P2<sup>[72]</sup>. The characteristics of each emission band depend upon whether it arises from a doubly charged vacancy center  $V_o^{++}$  (P2) or a singly charged vacancy center  $V_o^+$  (P1). The  $V_o^{++}$  center, created by capture of a hole by the  $V_o^+$  center in a depletion region, leads to the P2 emission line. The singly charged center ( $V_o^+$ ) in the absence of a depletion region turns into a neutral center ( $V_o^\times$ ) upon the capture of an electron (n-type ZnO) from the conduction band which then recombines with a hole in the valence band giving rise to the P1 emission<sup>[68]</sup>. The spectral content of the blue-green band is determined by the relative weight of the two overlapping emission peaks.

As shown in Figure 9b, when excitation below the band-gap ( $\lambda_{ex} = 375$  nm) was used, the defect-related emission is suppressed in the presence of Au NPs. Herein, we propose FRET from donor ZnO NP to Au acceptor, which is responsible for the observed suppression of emission bands. The mechanism of FRET involves a donor in an excited electronic state, which may transfer its excitation energy to a nearby acceptor in a nonradiative fashion through long range dipole-dipole interaction<sup>[66]</sup>. The theory is based on the concept of treating an excited donor as an oscillating dipole that can undergo energy exchange with a second dipole having similar resonance frequency. In principle, if the fluorescence emission spectrum of the donor molecule overlaps the absorption spectrum of an acceptor molecule, and the two are within a minimal distance from one another (1-10 nm), the donor can directly transfer its excitation energy to the acceptor via exchange of a virtual photon. The spectral overlap of the ZnO emission spectrum with that of the Au absorption spectrum is shown in Figure 10a. The faster excited state lifetime of the ZnO-Au NC with respect to that of the free ZnO NP is clearly noticeable from Figure 10b. Details of the spectroscopic parameters and the fitting parameters of the fluorescence decays are tabulated in Table 4. In order to estimate FRET efficiency of the donor (ZnO) and hence to determine distances of donor-acceptor pairs, we followed the methodology described in chapter 13 of reference<sup>[66]</sup>. In this case the spectral overlap integral,  $J$  (Equation 2) is found to be  $2.82 \times 10^{16}$ . From the average lifetime calculation for the ZnO-Au NC, we obtain the effective distance between the donor and the acceptor,  $r_{DA} \approx 2.55$  nm, using Equation 3 and 4. It is to be noted that the smaller value of  $r_{DA}$  compared to the radius of the ZnO NPs ( $\sim 3$  nm; Figure 7a) can be rationalized from the fact that the origin of the PL peaking at 550 nm arises essentially from surface defects in the ZnO NPs<sup>[71]</sup>. Moreover, comparing the PL spectra of bare ZnO NPs and ZnO-Au NCs upon excitation above the band-edge, it was observed that the emission due to excitonic recombination is suppressed, while the defect-related emission is red shifted in the presence of Au NPs. In this respect, we have shown that the energy is transferred from the  $V_o^+$  center to Au NPs which leads to a reduction in the PL intensity at 520 nm. The energy transfer efficiency ( $E$ ) is found to be  $\sim 19\%$  (Figure 8d) which is much lower value compared to that of below band-gap excitation ( $E = \sim 85\%$ ).

**Table 4:** Dynamics of picosecond-resolved luminescence transients of ZnO NPs in the presence and absence of Au NPs<sup>a</sup> and the kinetics parameters<sup>b</sup> for the photoselective degradation of Methylene Blue in the presence of ZnO and ZnO-Au nanocolloids

<b>DYNAMICS STUDY</b>				
<i>Samples</i>	$\tau_1$ (ns)	$\tau_2$ (ns)	$\tau_3$ (ns)	$\tau_{avg}$ (ns)
ZnO NP (bare)	47.58 (41%)	3.78 (23%)	0.280 (36%)	20.48
ZnO-Au NC	33.34 (8%)	2.60 (10%)	0.051 (82%)	2.97
<b>KINETICS STUDY [y=A exp(-kt) + y<sub>0</sub>]</b>				
<i>Samples and Filters</i>	$k$ (sec <sup>-1</sup> )	A (%)	$R^2$	
ZnO (420 HP)	$1.055 \times 10^{-3}$	2.66	0.9644	
ZnO-Au (420 HP)	$1.388 \times 10^{-3}$	2.78	0.9378	
ZnO (460 LP)	$2.203 \times 10^{-3}$	11.68	0.9704	
ZnO-Au (460 LP)	$2.528 \times 10^{-3}$	29.31	0.9961	
ZnO (320 HP-460 LP)	$2.340 \times 10^{-3}$	23.55	0.9939	
ZnO-Au (320 HP-460 LP)	$2.287 \times 10^{-3}$	19.65	0.9985	

<sup>a</sup>The emissions from ZnO NPs and ZnO-Au NCs (probing at 550 nm) were detected with a 375 nm laser excitation. Numbers in the parentheses indicate relative weightage.

<sup>b</sup>kinetic constants (k), regression coefficients ( $R^2$ ) and the percentages of photoselective degradation (A). Parentheses indicate the optical filters used in the study.

In retrospect, excited electrons are preferentially trapped by  $V_o^{++}$  center, which is originated by  $V_o^+$  by capturing a hole. The formation of  $V_o^{++}$  centers is more favourable upon band-edge excitation since the photogenerated holes have enough time to migrate during thermalization of highly excited electrons. This leads to more facile recombination of excited electrons via  $V_o^{++}$  centers, and this recombination pathway is supported by the appreciable red shift observed in ZnO-Au NCs upon above band-edge excitation. However, the decrease in band-edge emission intensity in the presence of Au NPs is well understood, whereby Au acts as a sink which can store and shuttle photogenerated electrons<sup>[54,83]</sup>. As per our understanding, the optical activity of surface defect states in the overall emission of the semiconductor solely depends on the excitation wavelength.

It was reported by several researchers that in the presence of metal NPs in close proximity to semiconductor NPs, enhanced photocatalytic degradation of test solutions was observed. Thus we compared the role of a Au layer in promoting photogenerated charges in ZnO–Au and ZnO colloids by carrying out photo-reduction of a test contaminant [MB, purchased from Carlo Erba]; MB is known to be an excellent probe for the study of interfacial electron transfer in colloidal semiconductor systems<sup>[15]</sup>. In general, the higher the charge migration from the surface of the ZnO semiconductor, the faster will be the degradation of the surface-attached MB. We have used a fiber-optic based system for the measurement of light-induced

chemical processes with spectroscopic precision. To demonstrate the sensitivity and usefulness of our designed system, we previously conducted a detailed study of the photodeterioration of vitamin B2 (riboflavin) in aqueous phase<sup>[84]</sup>. In order to obtain different excitations we have used three different types of filters placed on a home-made UV bath (60 W; normally used for water purification). The optical filters, namely 420 high pass (HP), 460 low pass (LP) and 320 high pass (HP), were chosen in order to achieve controlled and preferential excitation. The characteristics of the optical filters are shown in Figure 11a, which clearly depicts that 420 HP (passes light above 420 nm) is only used for the SP excitation of Au NPs, 460 LP (passes light below 460 nm) is used for the above band-edge excitation of ZnO, and the combined use of 320 HP and 460 LP (passes light above 320 nm and below 460 nm) leads to preferential excitation of below band-gap excitation of ZnO. In Figure 11b, the relative concentration ( $C_t/C_0$ ) of MB in solution is

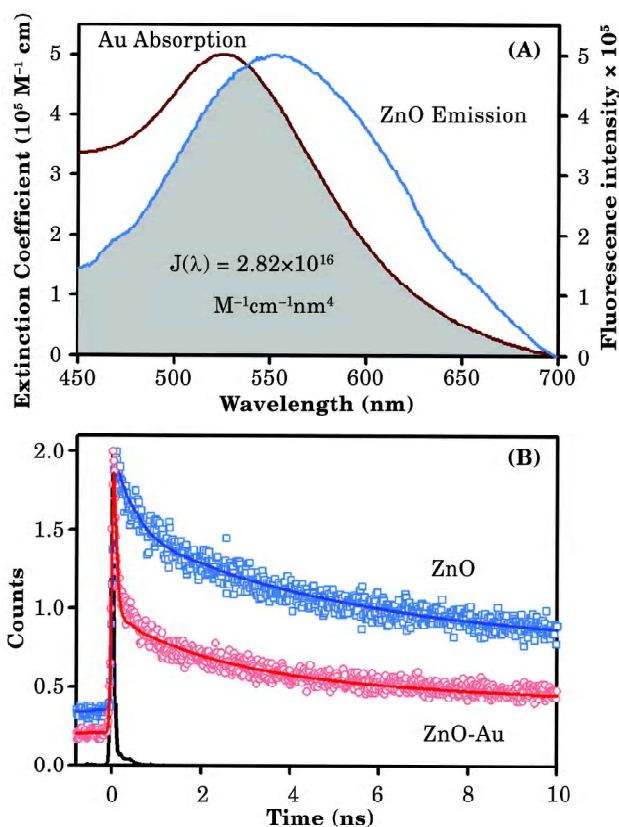


**Fig. 10:** (a) SP band of Au NPs and emission spectra of ZnO NPs are shown. An overlapping zone between emission of ZnO NPs and absorption of acceptor Au is indicated as a green shaded zone. (b) The picosecond-resolved fluorescence transients of ZnO NPs, in the absence (blue) and presence of acceptor Au (red) (excitation at 375 nm) collected at 550 nm.

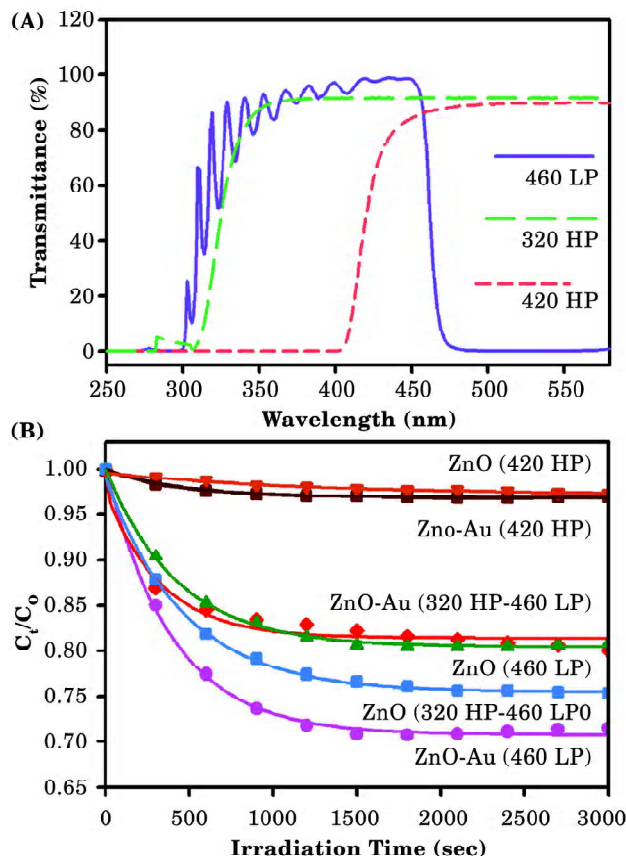


**Fig. 11:** (a) The transmittance spectra of 320 high pass (green), 420 high pass (red) and 460 low pass (violet) optical filters are shown. (b) Plot of relative concentration ( $C_t/C_0$ ) versus time for the degradation of MB (monitored at 655 nm) is shown. The degradation is performed in the presence of colloidal solutions of ZnO NPs and ZnO–Au NCs under different excitation conditions (Parentheses indicate the optical filters used for the desired excitation).

plotted with respect to UV irradiation time, the results of which indicate the photo degradation of MB upon continued UV irradiation. It is to be noted that there was no obvious change in the concentration of MB stored in the dark for several hours (data are not shown here). Under selective UV radiation we have recorded the absorption peak of MB (at 655 nm) at 5 second intervals, using SPECTRA SUITE software supplied by Ocean Optics, and plotted it against the time of photo irradiation. All the photo degradation curves were found to follow a first-order exponential equation, and the kinetic parameters are represented in Table 4. The decrease in the absorbance at 655 nm implies the generation of the colourless photoproduct Leuco-Methylene Blue (LMB). Note that in the present study we are interested in exploring the long-time photo degradation of MB (for several

minutes). To compare the photo degradation of MB in the presence of ZnO NPs and ZnO–Au NCs with a 420 HP filter, it is clearly shown that no considerable change in absorbance peak at 655 nm takes place upon Au SP excitation. The photo degradation rates are found to be  $1.055 \times 10^{-3} \text{ sec}^{-1}$  and  $1.388 \times 10^{-3} \text{ sec}^{-1}$ , and the percentages of total photo degradation (i.e., the value of A in the first-order kinetic equation shown in Table 4) are 2.66 and 2.78 for ZnO and ZnO–Au NCs, respectively. It reveals that electron transfer from Au NPs to MB is not allowed upon direct excitation of Au. Upon, replacing the 420 HP filter with a 460 LP filter, we observed an increase in the photo degradation rates in the presence of Au NPs ( $k_{\text{ZnO}} = 2.203 \times 10^{-3} \text{ sec}^{-1}$ ,  $k_{\text{ZnO–Au}} = 2.258 \times 10^{-3} \text{ sec}^{-1}$ ), and the percentage of photo degradation also improved from  $A_{\text{ZnO}} = 11.68$  to  $A_{\text{ZnO–Au}} = 29.31$ . This is attributed to improved charge separation in the presence of Au NPs which also can store and shuttle excited electrons, thereby suppressing recombination. Such Au NP–stabilized ZnO NPs behave as more efficient electron accumulators (at the conduction band) than the bare oxide<sup>[36]</sup>. In retrospect, the photo degradation rate of MB was observed to decrease ( $k_{\text{ZnO}} = 2.340 \times 10^{-3}$ ,  $k_{\text{ZnO–Au}} = 2.287 \times 10^{-3}$ ), and the percentage of total photo degradation was found to be much lower ( $A_{\text{ZnO}} = 23.55$ ,  $A_{\text{ZnO–Au}} = 19.65$ ) in the presence of Au NPs when we used combined optical filters of 320 HP and 460 LP. This happens because excited electrons of ZnO can easily occupy the defect centers and resonantly transfer their energy to Au NPs via non-radiative processes (FRET, as previously discussed). As a consequence, in presence of Au, excited electrons are unable to migrate from the ZnO surface to perform the reduction of MB. Thus, it is important to note that the differences in rate constants are not significant, whereas considerable differences in the magnitude of total photo degradation are observed during above band-edge and below band-gap excitation of ZnO and ZnO–Au NCs. This is due to the fact that the total number of active electrons available for carrying out MB degradation is different for ZnO and ZnO–Au NCs for any particular excitation. Our study clearly demonstrates that the role of incorporated metal on semiconductor for facilitating redox reactions is solely dependent on the excitation of the semiconductor.

The efficient charge migration in metal-semiconductor NCs is expected to lead to improved DSSC performance of ZnO–Au NCs compared to bare ZnO<sup>[85]</sup>. Thus, we measured and directly compared the IPCE (using Equation 7) of ZnO and ZnO–Au based DSSCs. Each of the two examined ZnO and ZnO–Au–based cells contained the same sensitizer dye N719 and  $\text{I}^-/\text{I}_3^-$  electrolyte, to allow for a fair comparison. The IPCE curves of the two cells are presented in Figure 12a which shows a broad spectral response in the range 440 to 600 nm. Significant enhancement in photocurrent generation is seen upon deposition of Au NPs on the ZnO electrodes. The enhancement in the photocurrent generation efficiency is indicative of the fact that the Au NPs assist in the charge separation within the nanostructured ZnO film as well as improve the interfacial charge transfer processes. Figure

12b shows the photocurrent-voltage ( $J$ - $V$ ) characteristics for solar cells, constructed using the bare ZnO NPs and ZnO-Au NCs. The short-circuit current density ( $J_{sc}$ ) and the open-circuit voltage ( $V_{oc}$ ) of the ZnO-Au NC-based DSSC were  $261.87 \mu\text{A}/\text{cm}^2$  and  $0.605 \text{ V}$ , respectively, which are much higher than that of the bare ZnO-based DSSC ( $J_{sc} = 7.5 \mu\text{A}/\text{cm}^2$ ,  $V_{oc} = 0.394 \text{ V}$ ). The calculated values of FF and the overall power conversion efficiency of the ZnO-based DSSC were 30% and 0.012%, respectively, which are substantially improved in the presence of gold (FF = 53% and  $\eta = 0.8\%$ ). Table 5 summarizes the measured and calculated values obtained from each  $J$ - $V$  curve. The photoconductivity measurement<sup>[86-87]</sup> of the ZnO NP and ZnO-Au NC thin films were necessary in order to further understand the electron mobility (*i.e.* performance of the semiconductor) and charge transfer mechanism. At a fixed bias voltage of  $5 \text{ V}$ , the photocurrent across the thickness of the thin films was measured by using FTO as one of the

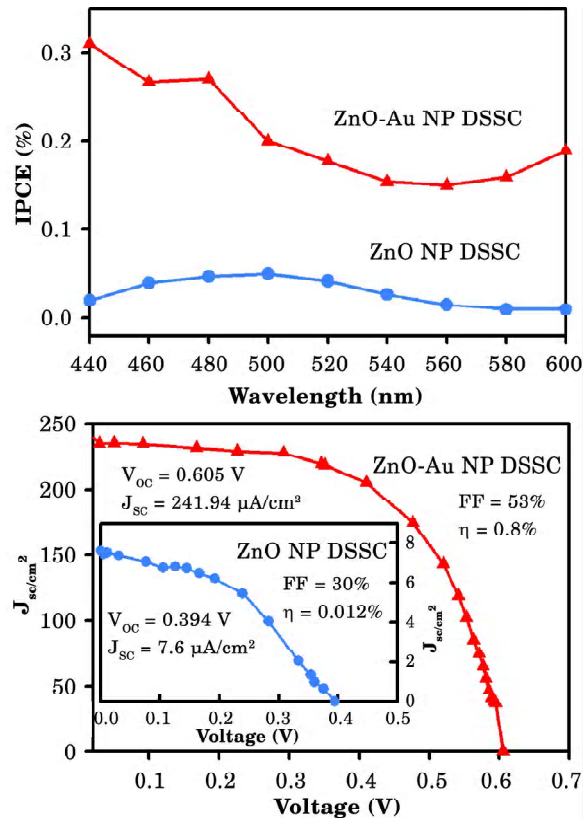


**Fig. 12:** (a) Dependence of the incident photon conversion efficiency on the incident wavelength for ZnO NP (blue) and ZnO-Au NC (red) films cast on an FTO plate. (b) Photocurrent-voltage ( $J$ - $V$ ) characteristics of ZnO-Au NC and ZnO NP (inset) based DSSC (with  $10.5 \text{ klux}$  illumination intensity at the area of  $0.16 \text{ cm}^2$  from a  $90 \text{ W}$  xenon lamp).

**Table 5:** Device performance<sup>a</sup> of the dye-sensitized solar cells with ZnO NP and ZnO–Au NC

<i>Device with N719</i>	$V_{oc}$ (V)	$J_{sc}$ ( $\mu A/cm^2$ )	FF (%)	$\eta$ (%)
ZnO NP	0.394	7.5	44	0.012
ZnO–Au NC	0.605	261.87	53	0.8

<sup>a</sup>short circuit photocurrent densities ( $J_{sc}/cm^2$ ), open-circuit voltage ( $V_{oc}$ ), fill factor (FF), and efficiency ( $\eta$ ) (See Equation 8–9).

electrodes and a small (4 mm diameter) drop of mercury (Hg) on top of the film as a counter electrode. The light source (intensity 25 mW/cm<sup>2</sup>) was turned ON and OFF every 20 seconds, and the obtained current values were continuously recorded using a programmable multimeter (Gwinstek GDM–396). Figure 13 shows the photocurrent response for the ZnO NP and ZnO–Au NC thin films, where an improved photocurrent was observed for the ZnO–Au NC thin film (~70  $\mu A$ ) under illuminated condition compared to the ZnO NP thin film (~1.5  $\mu A$ ).

This shows that the photogenerated electrons in ZnO NPs (from visible light absorption by the intermediate  $Vo^+$  center) are transferred to Au NPs, as mentioned earlier contributing in enhanced photocurrent of the ZnO–Au NC thin films compared to the ZnO NP. In case of the model DSSC shown here, a similar mechanism is responsible for the enhanced photocurrent observed (Figure 12b) in the presence of Au NPs along with the ZnO NPs. Some of the injected electrons from the excited N719 dye to

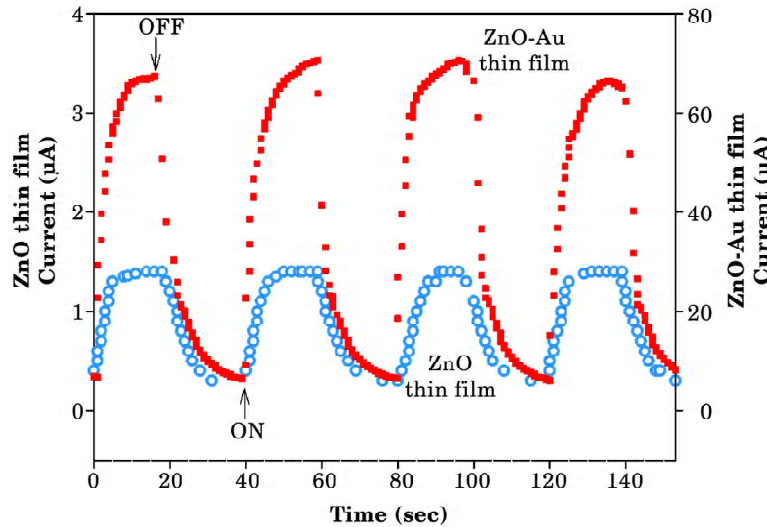
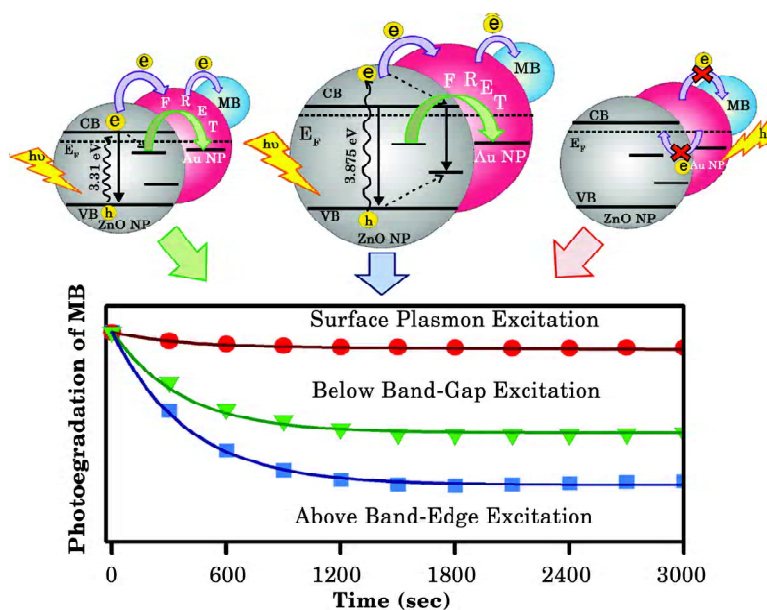


**Fig. 13:** Photocurrent responses of ZnO NP and ZnO–Au NC thin films under bias voltage of 5V. The photocurrent was measured across the thickness of the films with 25 mW/cm<sup>2</sup> incident power from a halogen light source.

the CB of ZnO are captured by the intermediate defect sites of ZnO ( $\text{Vo}^+$ ) resulting in poor photocurrent and fill factor of DSSC. However, in the presence of Au NPs in the ZnO thin film, we have observed higher photocurrent ( $J_{\text{sc}} = 261.87 \mu\text{A}/\text{cm}^2$ ) and fill factor ( $\text{FF} = 53\%$ ) compared to the ZnO NP DSSC ( $J_{\text{sc}} = 7.5 \mu\text{A}/\text{cm}^2$  and  $\text{FF} = 44\%$ ). Thus, it is noted that the ratios of improved photocurrent response (70:1.5) and short circuit current (261.9:7.5) for ZnO and ZnO–Au semiconductors are comparable. The improvement observed in the overall device performance is mainly due to increased conductivity by transferring the trapped electrons in  $\text{Vo}^+$  centers of ZnO to Au NPs which then contribute to the photocurrent as well as the fill factor of the DSSC. It is worth noting that the efficiency obtained from the model DSSC with the use of NPs is lower than the maximum efficiency reported<sup>[38]</sup> with NRs, which were employed to provide higher surface area and better charge transport. The overall mechanistic explanation for the excitation-dependent recombination processes and the catalytic activity of Au NPs in the ZnO–Au NCs, as schematically shown in Scheme 3.



**Scheme 3:** Schematic representation of the metal-semiconductor system: The system consists of a semiconductor ZnO NP (gray big ball) containing appreciable amounts of defect states on which a Au NP (red big ball) is fabricated. Methylene Blue (small blue ball) is bound to the ZnO–Au NC by surface adsorption. The dynamics of charge separation and interparticle charge/energy migration of the entire structure is shown. Thereafter, photo degradation of Methylene Blue under different excitation conditions is also shown by a graph which reveals the mediating role of Au NP in photocatalysis.

#### 4. CONCLUSION

In summary, we have explored the dynamics of light harvesting of ZnO NPs in the near infrared region. We have shown that at the emission peak (550 nm) of the ZnO NP–Oxazine 1 adduct, efficient FRET (~93%) occurs from surface state emission to the acceptor Oxazine 1 chromophore. The overall picture that evolved from our studies is summarized in scheme 1. Comparatively less efficient (63%) dynamics of the light harvesting of the ZnO NPs from the emission peaking at 495 nm, arises due to the defect sites located within the bulk of the NPs. This can be separated from that of the emission obtained at 550 nm which originates from below band gap emission at the surface of the NPs. It is to be noted that the FRET distance ( $r_{DA}$ ) is dependent on the emission wavelength of ZnO NPs whether it arises from surface or near bulk states. Therefore,  $r_{DA}$  can be interpreted as a parameter that signifies the distance between the probe (OX1) and the different vacancy states of ZnO NPs. The possibility of the electron transfer reaction is ruled out from the picoseconds–resolved fluorescence decay of the acceptor OX1 molecules at the ZnO surface. We have also shown that the efficiency of the ZnO NPs as light harvesting material is much higher (efficiency 93%) than that of the NRs. Our experimental observations may find relevance in the light harvesting devices using ZnO NPs.

Subsequently, time correlated single photon counting spectroscopy was carried out to understand the resonance energy transfer phenomenon in a ZnO/N719 system which is extensively used in DSSCs. The semiconductor ZnO NPs was found to transfer the excited state energy to SD N719 at the surface of the NPs. The observed energy transfer in presence of high energy photons leads to significant increase the short circuit current ( $43.86 \pm 8\%$ ) in ZnO based DSSC leading to more than 50% increased energy conversion efficiency.  $TiO_2$  based solar cell showed marginal increase in short circuit current and a slight efficiency improvement (~10%). The possibility of the back electron transfer from the ZnO surface to the N719 has also been compared by studying the complexation of the NPs with an electron accepting organic molecule BQ. It has been found that the energy transfer process does not involve the physical migration of electron from the surface of the excited ZnO to the SD. Our studies may find relevance in the enhancement of harvesting of high energy photon by semiconductors with defect centers without further addition of co-sensitizer in a DSSC. The observed FRET dynamics in the light harvesting process opens the way toward the utilization of new materials which contains appreciable amount of defect states. These findings provide the importance of the various semiconductors containing inherent optical defect centres and how the defect centres can be beneficially utilized for light harvesting/sensitization.

Finally, our studies also provide a mechanistic explanation for the excitation-dependent recombination processes and the catalytic activity of

Au NPs in the ZnO–Au NCs, as schematically shown in Scheme 3. A better understanding of the charge-transfer processes at the semiconductor/metal interface is crucial for optimizing the performance of such catalysts. Our results demonstrate that the excited ZnO NPs resonantly transfer visible optical radiation to the Au NPs upon below band-gap excitation of the semiconductor. A singly charged vacancy center of the ZnO semiconductor is demonstrated to be responsible for the visible optical radiation transfer from ZnO NPs to Au NPs, whereas, a combination of the energy transfer between surface defects and SP of Au NPs, as well as thermalization of photogenerated electron-hole pair and their recombination in the ZnO NPs is believed to take place simultaneously upon above band-edge excitation. We observe that the prepared ZnO–Au NCs are stable and efficient enough for the environmental purification of organic pollutants. As a low-cost photovoltaic cell, the incident photon-to-current conversion efficiency and short-circuit current is significantly improved in presence of Au NPs which is attributed to the better electron mobility of the ZnO–Au NCs. This approach may give rise to a new class of multifunctional materials with possible applications in energy-conversion devices and biofunctionalized materials.

#### ACKNOWLEDGEMENTS

SS thanks UGC, AM thanks CSIR. We thank DST for financial grants SR/SO/BB-15/2007.

#### REFERENCES

- [1] Duysens, L. (1964). Photosynthesis. *Prog. Biophys. Mol. Biol.*, 14: 101–104.
- [2] Cheng, Y.C. and Fleming, G.R. (2009). Dynamics of Light Harvesting in Photosynthesis. *Annu. Rev. Phys. Chem.*, 60: 241–262.
- [3] Grätzel, M. (2004). Conversion of Sunlight to Electric Power by Nanocrystalline Dye-Sensitized Solar Cells. *J. Photochem. and Photobiol. A.*, 164: 3–14.
- [4] Kamat, P.V. (2008). Quantum Dot Solar Cells. Semiconductor Nanocrystals as Light Harvesters. *J. Phys. Chem. C.*, 112: 18737–18753.
- [5] Narayanan, S.S., Sinha, S.S., Verma, P.K. and Pal, S.K. (2008). Ultrafast Energy Transfer from 3-Mercaptopropionic Acid-Capped CdSe/ZnS QDs to Dye-Labelled DNA. *Chem. Phys. Lett.*, 463: 160–165.
- [6] Banerjee, D. and Pal, S.K. (2007). Simultaneous Binding of Minor Groove Binder and Intercalator to Dodecamer DNA: Importance of Relative Orientation of Donor and Acceptor in FRET. *J. Phys. Chem. B.*, 111: 5047–5052.
- [7] Narayanan, S.S., Sinha, S.S. and Pal, S.K. (2008). Sensitized Emission from a Chemotherapeutic Drug Conjugated to CdSe/ZnS QDs. *J. Phys. Chem. C.*, 112: 12716–12720.
- [8] Scheller, F.W., Wollenberger, U., Warsinke, A. and Lisdat, F. (2001). Research and Development in Biosensors. *Curr. Opin. Biotechnol.*, 12: 35–40.
- [9] Morrison, L.E. (1988). Basic Principles of Fluorescence and Energy Transfer. *Anal. Biochem.*, 174: 101–120.

- [10] Ha, T., Enderle, T., Ogletree, D.F., Chemla, D.S., Selvin, P.R. and Weiss, S. (1996). Probing the interaction between two single molecules: fluorescence resonance energy transfer between a single donor and a single acceptor. *Proc. Natl. Acad. Sci. U. S. A.*, 93: 6264–6268.
- [11] Iqbal, S.S., Mayo, M.W., Bruno, J.G., Bronk, B.V., Batt, C.A. and Chambers, J.P. (2000). A Review of Molecular Recognition Technologies for Detection of Biological Threat Agents. *Biosens. Bioelectron.*, 15: 549–578.
- [12] Whitcombe, D., Theaker, J., Guy, S.P., Brown, T. and Little, S. (1999). Detection of PCR Products Using Self-Probing Amplicons and Fluorescence. *Nat. Biotechnol.*, 17: 804–807.
- [13] Cardullo, R.A., Agrawal, S., Flores, C., Zamecnik, P.C. and Wolf, D.E. (1988). Detection of Nucleic Acid Hybridization by Nonradiative Fluorescence Resonance Energy Transfer. *Proc. Natl. Acad. Sci. U.S.A.*, 85: 8785–8789.
- [14] Law, M., Greene, L.E., Johnson, J.C., Saykally, R. and Yang, P. (2005). Nanowire Dye-Sensitized Solar Cells. *Nat. Mater.*, 4: 455–459.
- [15] Baruah, S., Sinha, S.S., Ghosh, B., Pal, S.K., Raychaudhuri, A.K. and Dutta, J. (2009). Photoreactivity of ZnO Nanoparticles in Visible Light: Effect of Surface States on Electron Transfer Reaction. *J. Appl. Phys.*, 105: 074308.
- [16] Sarkar, S., Makhal, A., Baruah, S., Mahmood, M.A., Dutta, J. and Pal, S.K. (2012). Nanoparticle-Sensitized Photo degradation of Bifenthrin and Potential Therapeutic Application. *J. Phys. Chem. C.*, 116: 9608–9615.
- [17] Pal, S.K., Mandal, D., Sukul, D. and Bhattacharyya, K. (1999). Photoinduced Electron Transfer Between Dimethylaniline and Oxazine 1 in Micelles. *Chem. Phys.*, 249: 63–71.
- [18] Grätzel, M. (2001). Photoelectrochemical Cells. *Nature*, 414: 338–344.
- [19] O'Regan, B. and Grätzel, M. (1991). A Low-Cost, High-Efficiency Solar Cell Based on Dye-Sensitized Colloidal TiO<sub>2</sub> Films. *Nature*, 353: 737–740.
- [20] Bai, Y., Cao, Y., Zhang, J., Wang, M., Li, R., Wang, P., Zakeeruddin, S.M. and Grätzel, M. (2008). High-Performance Dye-Sensitized Solar Cells Based on Solvent-Free Electrolytes Produced from Eutectic Melts. *Nat. Mater.*, 7: 626–630.
- [21] Shankar, K., Feng, X. and Grimes, C.A. (2009). Enhanced Harvesting of Red Photons in Nanowire Solar Cells: Evidence of Resonance Energy Transfer. *ACS Nano*, 3: 788–794.
- [22] Ferrere, S., Zaban, A. and Gregg, B.A. (1997). Dye Sensitization of Nanocrystalline Tin Oxide by Perylene Derivatives. *J. Phys. Chem. B.*, 101: 4490–4493.
- [23] Sayama, K., Sugihara, H. and Arakawa, H. (1998). Photoelectrochemical Properties of a Porous Nb<sub>2</sub>O<sub>5</sub> Electrode Sensitized by a Ruthenium Dye. *Chem. Mater.*, 12: 3825–3832.
- [24] Kruger, J., Plass, R., Gratzel, M., Cameron, P.J. and Peter, L.M. (2003). Charge Transport and Back Reaction in Solid State Dye-Sensitized Solar Cells: A Study using Intensity-Modulated Photovoltage and Photocurrent Spectroscopy. *J. Phys. Chem. B.*, 107: 7536–7539.
- [25] Nazeeruddin, M.K., Angelis, F.D., Fantacci, S., Selloni, A., Viscardi, G., Liska, P., Ito, S., Takeru, B. and Grätzel, M. (2005). Combined Experimental and DFT-TDDFT Computational Study of Photoelectrochemical Cell Ruthenium Sensitizers. *J. Am. Chem. Soc.*, 127: 16835–16847.
- [26] Hamman, T.W., Jensen, R.A., Martinson, A.B.F., Ryswyk, H.V. and Hupp, J.T. (2008). Advancing Beyond Current Generation Dye-Sensitized Solar Cells. *Energy Environ. Sci.*, 1: 66–78.
- [27] Wang, P., Zakeeruddin, S.M., Moser, J.E., Nazeeruddin, M.K., Sekiguchi, T. and Grätzel, M. (2003). A Stable Quasi-Solid-State Dye-Sensitized Solar Cell with an Amphiphilic Ruthenium Sensitizer and Polymer Gel Electrolyte. *Nat. Mater.*, 2: 402–407.

- [28] Yum, J.H., Walter, P., Huber, S., Rentsch, D., Geiger, T., Nüesch, F. Angelis, F.D., Grätzel, M. and Nazeeruddin, M.K. (2007). Efficient Far Red Sensitization of Nanocrystalline  $\text{TiO}_2$  Films by an Unsymmetrical Squaraine Dye. *J. Am. Chem. Soc.*, 129: 10320–10321.
- [29] Hardin, B.E., Hoke, E.T., Armstrong, P.B., Yum, J.H., Comte, P., Torres, T., Frechet, J.M.J., Nazeeruddin, M.K., Grätzel, M. and McGehee, M.D. (2009). Increased Light Harvesting in Dye–Sensitized Solar Cells with Energy Relay Dyes. *Nat. Photonics*, 3: 406–411.
- [30] Cid, J.J., Yum, J.H., Jang, S.R., Nazeeruddin, M.K., Martinez–Ferrero, E., Palomares, E., Ko, J., Gratzel, M. and Torres, T. (2007). Molecular Cosensitization for Efficient Panchromatic Dye–Sensitized Solar Cells. *Angew. Chem. Int. Ed.*, 119: 8510–8514.
- [31] Siegers, C., Hohl–Ebinger, J., Zimmermann, B., Würfel, U., Mülhaupt, R., Hinsch, A. and Haag, R. (2007). A Dyadic Sensitizer for Dye Solar Cells with High Energy Transfer Efficiency in the Device. *Chem. Phys. Chem.*, 8: 1548–1556.
- [32] Keis, K., Bauer, C., Boschloo, G., Hagfeldt, A., Westermark, K., Rensmo, H. and Siegbahn, H. (2002). Nanostructured ZnO Electrodes for Dye–Sensitized Solar Cell Applications. *J. Photochem. Photobiol. A: Chemistry*, 148: 57–64.
- [33] Suh, D.I., Lee, S.Y., Kim, T.H., Chun, J.M., Suh, E.K., Yang, O.B. and Lee, S.K. (2007). The Fabrication and Characterization of Dye–Sensitized Solar Cells with a Branched Structure of ZnO Nanowires. *Chem. Phys. Lett.*, 442: 348–353.
- [34] Rao, A.R. and Dutta, V. (2008). Achievement of 4.7% Conversion Efficiency in ZnO Dye–Sensitized Solar Cells Fabricated by Spray Deposition using Hydrothermally Synthesized Nanoparticles. *Nanotechnology*, 19: 445712.
- [35] Yang, P., Yan, H., Mao, S., Russo, R., Johnson, J., Saykally, R., Morris, N., Pham, J., He, R. and Choi, H. (2002). Controlled Growth of ZnO Nanowires and Their Optical Properties. *J. Adv. Func. Mater.*, 12: 323–331.
- [36] Xia, J.B. and Zhang, X.W. (2006). Electronic Structure of ZnO Wurtzite Quantum Wire. *Eur. Phys. J. B.*, 49: 415–420.
- [37] Quintana, M., Edvinsson, T., Hagfeldt, A. and Boschloo, G. (2007). Comparison of Dye–Sensitized ZnO and  $\text{TiO}_2$  Solar Cells: Studies of Charge Transport and Carrier Lifetime. *J. Phys. Chem. C.*, 111: 1035–1041.
- [38] Keis, K., Magnusson, E., Lindstrom, H., Lindquist, S.E. and Hagfeldt, A. (2002). A 5% Efficient Photoelectrochemical Solar Cell Based on Nanostructured ZnO Electrodes. *Sol. Energy Mater. Sol. Cells*, 73: 51–58.
- [39] Murray, C.B., Kagan, C.R. and Bawendi, M.G. (1995). Self–Organization of CdSe Nanocrystallites into Three–Dimensional Quantum Dot Superlattices. *Science*, 270: 1335–1338.
- [40] Henglein, A. (1989). Small–Particle Research: Physicochemical Properties of Extremely Small Colloidal Metal and Semiconductor Particles. *Chem. Rev.*, 89: 1861–1873.
- [41] Olson, T.Y. and Zhang, J.Z. (2008). Structural and Optical Properties and Emerging Applications of Metal Nanomaterials. *J. Mater. Sci. Technol.*, 24: 433–446.
- [42] Sliem, M.A., Hikov, T., Li, Z.A., Spasova, M., Farle, M., Schmidt, D.A., Newen, M.H. and Fischer, R.A. (2010). Interfacial Cu/ZnO Contact by Selective Photodeposition of Copper onto the Surface of Small ZnO Nanoparticles in Non–Aqueous Colloidal Solution. *Phys. Chem. Chem. Phys.*, 12: 9858–9866.
- [43] Fang, X.S., Zhai, T.Y., Gautam, U.K., Li, L., Wu, L.M., Bando, Y. and Golberg, D. (2011). ZnS Nanostructures: From Synthesis to Applications. *Prog. Mater. Sci.*, 56: 175–287.
- [44] Link, S. and El–Sayed, M.A. (1999). Spectral Properties and Relaxation Dynamics of Surface Plasmon Electronic Oscillations in Gold and Silver Nanodots and Nanorods. *J. Phys. Chem. B.*, 103: 8410–8426.

- [45] Jin, R., Cao, Y.C., Mirkin, C.A., Kelly, K.L., Schatzand, G.C. and Zheng, J.G. Photoinduced Conversion of Silver Nanospheres to Nanoprisms. *Science*, 294: 1901–1903. 
- [46] Kamat, P.V. (2002). Photophysical, Photochemical and Photocatalytic Aspects of Metal Nanoparticles. *J. Phys. Chem. B.*, 106: 7729–7744.
- [47] Valden, M.; Lai, X. and Goodman, D.W. (1998). Onset of Catalytic Activity of Gold Clusters on Titania with the Appearance of Nonmetallic Properties. *Science*, 281: 1647–1650.
- [48] Haruta, M. (1997). Size and Support–Dependency in the Catalysis of Gold. *Catal. Today*, 36: 153–166.
- [49] Chen, Z.H., Tang, Y.B., Liu, C.P., Leung, Y.H., Yuan, G.D., Chen, L.M., Wang, Y.Q., Bello, I., Zapien, J.A., Zhang, W.J., Lee, C.S. and Lee, S.T. (2009). Vertically Aligned ZnO Nanorod Arrays Sentsized with Gold Nanoparticles for Schottky Barrier Photovoltaic Cells. *J. Phys. Chem. C* 113: 13433–13437.
- [50] Tian, Y. and Tatsuma, T. (2005). Mechanisms and Applications of Plasmon–Induced Charge Separation at TiO<sub>2</sub> Films Loaded with Gold Nanoparticles. *J. Am. Chem. Soc.*, 127: 7632–7637.
- [51] Subramanian, V., Wolf, E.E. and Kamat, P.V. (2001). Semiconductor–Metal Composite Nanostructures. To What Extent Do Metal Nanoparticles Improve the Photocatalytic Activity of TiO<sub>2</sub> Films? *J. Phys. Chem. B.*, 105: 11439–11446.
- [52] Chandrasekharan, N. and Kamat, P.V. (2000). Improving the Photoelectrochemical Performance of Nanostructured TiO<sub>2</sub> Films by Adsorption of Gold Nanoparticles. *J. Phys. Chem. B.*, 104: 10851–10857.
- [53] Wood, A., Giersig, M. and Mulvaney, P. (2001). Fermi Level Equilibration in Quantum Dot–Metal Nanojunctions. *J. Phys. Chem. B.*, 105: 8810–8815.
- [54] Subramanian, V., Wolf, E.E. and Kamat, P.V. (2003). Green Emission to Probe Photoinduced Charging Events in ZnO–Au Nanoparticles. Charge Distribution and Fermi–Level Equilibration. *J. Phys. Chem. B.*, 107: 7479–7485.
- [55] Jakob, M. and Levanon, H. (2003). Charge Distribution between UV–Irradiated TiO<sub>2</sub> and Gold Nanoparticles: Determination of Shift in the Fermi Level. *Nano Lett.*, 3: 353–358.
- [56] Li, C., Li, L., Du, Z., Yu, H., Xiang, Y., Li, Y., Cai, Y. and Wang, T. (2008). Rapid and Ultrahigh Ethanol Sensing Based on Au–Coated ZnO Nanorods. *Nanotechnology*, 19: 035501.
- [57] Shibahara, K., Kuroda, N., Nishino, S. and Matsunami, H. (1987). Fabrication of p–n Junction Diodes Using Homoepitaxially Grown 6H–SiC at Low Temperature by Chemical Vapor Deposition. *Jpn. J. Appl. Phys.*, 26: 1815–1817.
- [58] Heo, Y.W., Norton, D.P. and Pearton, S.J. (2005). Origin of Green Luminescence in ZnO Thin Film Grown by Molecular–Beam Epitaxy. *J. Appl. Phys.*, 98: 073502.
- [59] Lin, C.C., Chen, H.P., Liao, H.C. and Chen, S.Y. (2005). Enhanced Luminescent and Electrical Properties of Hydrogen–Plasma ZnO Nanorods Grown on Wafer–Scale Flexible Substrates. *Appl. Phys. Lett.*, 86: 183103–183105.
- [60] Ohashi, N., Ishigaki, T., Okada, N., Sekiguchi, T., Sakaguchi, I. and Haneda, H. (2002). Effect of Hydrogen Doping on Ultraviolet Emission Spectra of Various Types of ZnO. *Appl. Phys. Lett.*, 80: 2869.
- [61] Lin, J.M., Lin, H.Y., Cheng, C.L. and Chen, Y.F. (2006). Giant Enhancement of Bandgap Emission of ZnO Nanorods by Platinum Nanoparticles. *Nanotechnology*, 17: 4391–4394.
- [62] Cheng, C.W., Sie, E.J., Liu, B., Huan, C.H.A., Sum, T.C., Sun, H.D. and Fan, H.J. (2010). Surface Plasmon Enhanced Band Edge Luminescence of ZnO Nanorods by Capping Au Nanoparticles. *Appl. Phys. Lett.*, 96: 071107.
- [63] Baruah, S., Thanachayanont, C. and Dutta, J. (2008). Growth of ZnO Nanowires on Nonwoven Polyethylene Fibers. *Sci. Technol. Adv. Mater.*, 9: 025009.

- [64] Sugunan, A., Warad, H.C., Boman, M. and Dutta, J. (2006). Zinc Oxide Nanowires in Chemical Bath on Seeded Substrates: Role of Hexamine. *J. Sol-Gel Sci. Technol.*, 39: 49–56.
- [65] Baruah, S. and Dutta, J. (2009). Hydrothermal Growth of ZnO Nanostructures. *Sci. Technol. Adv. Mater.*, 10: 013001.
- [66] Lakowicz, J.R. (1999). *Principles of Fluorescence Spectroscopy*. 2nd ed.; Kluwer Academic/Plenum Publishers,
- [67] Shalish, I., Temkin, H. and Narayanmurti, V. (2004). Size-Dependent Surface Luminescence in ZnO Nanowires. *Phys. Rev. B.*, 69: 245401.
- [68] Ghosh, M. and Raychaudhuri, A.K. (2008). Shape transition in ZnO nanostructures and its effect on blue-green photoluminescence. *Nanotechnology*, 19: 445704.
- [69] Tang, Y.B., Chen, Z.H., Song, H.S., Lee, C.S., Cong, H.T., Cheng, H.M., Zhang, W.J., Bello, I. and Lee, S.T. (2008). Vertically Aligned p-Type Single-Crystalline GaN Nanorod Arrays on n-Type Si for Heterojunction Photovoltaic Cells. *Nano Lett.*, 8: 4191–4195.
- [70] Beek, W.J.E., Wienk, M.M. and Janssen, R.A.J. (2006). Hybrid Solar Cells from Regioregular Polythiophene and ZnO Nanoparticles. *Adv. Funct. Mater.*, 16: 1112–1116.
- [71] Makhil, A., Sarkar, S., Bora, T., Baruah, S., Dutta, J., Raychaudhuri, A.K. and Pal, S.K. (2010). Dynamics of Light Harvesting in ZnO Nanoparticles. *Nanotechnology*, 21: 265703.
- [72] Ye, J.D., Gu, S.L., Qin, F., Zhu, S.M., Liu, S.M., Zhou, X., Liu, W., Hu, L.Q., Zhang, R., Shi, Y. and Zheng, Y.D. (2005). Correlation Between Green Luminescence and Morphology Evolution of ZnO Films. *Appl. Phys. A.*, 81: 759–762.
- [73] Dijken, A.V., Meulenkaamp, E.A., Vanmaekelbergh, D. and Meijerink, A. (2000). The Luminescence of Nanocrystalline ZnO Particles: The Mechanism of the Ultraviolet and Visible Emission. *J. Lumin.*, 87–89: 454–456.
- [74] Vanheusden, K., Warren, W.L., Seager, C.H., Tallant, D.R. and Voigt, J.A. (1996). Mechanisms Behind Green Photoluminescence in ZnO Phosphor Powders. *J. Appl. Phys.*, 79: 7983.
- [75] Jiang, C.Y., Sun, X.W., Lo, G.Q. and Kwong, D.L. (2007). Improved Dye-Sensitized Solar Cells with a ZnO-Nanowire Photoanode. *Appl. Phys. Lett.*, 90: 263501.
- [76] Zheng, Y., Chen, C., Zhan, Y., Lin, X., Zheng, Q., Wei, K., Zhu, J. and Zhu, Y. (2007). Luminescence and Photocatalytic Activity of ZnO Nanocrystals: Correlation between Structure and Property. *Inorg. Chem.*, 46: 6675–6682.
- [77] Shirota, H., Pal, H., Tominaga, K. and Yoshihara, K. (1998). Ultrafast Intermolecular Electron Transfer in Coumarin-Hydrazine System. *Chem. Phys.*, 236: 355–364.
- [78] Makhil, A., Sarkar, S., Bora, T., Baruah, S., Dutta, J., Raychaudhuri, A.K. and Pal, S.K. (2010). Role of Resonance Energy Transfer in Light Harvesting of Zinc Oxide-Based Dye-Sensitized Solar Cells. *J. Phys. Chem. C.*, 114: 10390–10395.
- [79] Burda, C., Green, T.C., Link, S. and El-Sayed, M.A. (1999). Electron Shuttling Across the Interface of CdSe Nanoparticles Monitored by Femtosecond Laser Spectroscopy. *J. Phys. Chem. B.*, 103: 1783–1788.
- [80] Makhil, A., Yan, H., Lemmens, P. and Pal, S.K. (2010). Light Harvesting Semiconductor Core-Shell Nanocrystals: Ultrafast Charge Transport Dynamics of CdSe-ZnS Quantum Dots. *J. Phys. Chem. C.*, 114: 627–632.
- [81] Sarkar, S., Makhil, A., Bora, T., Baruah, S., Dutta, J. and Pal, S.K. (2011). Photosensitive Excited State Dynamics in ZnO-Au Nanocomposites and their Implications in Photocatalysis and Dye-Sensitized Solar Cells. *Phys. Chem. Chem. Phys.*, 13: 12488–12496.
- [82] Haase, M., Weller, H. and Henglein, A. (1988). Photochemistry and Radiation Chemistry of Colloidal Semiconductors. 23. Electron Storage on Zinc Oxide Particles and Size Quantization. *J. Phys. Chem.*, 92: 482–487.

- [83] Subramanian, V., Wolf, E.E. and Kamat, P.V. (2004). Catalysis with TiO<sub>2</sub>/Gold Nanocomposites. Effect of Metal Particle Size on the Fermi Level Equilibration. *J. Am. Chem. Soc.*, 126: 4943–4950.
- [84] Sinha, S.S., Verma, P.K., Makhil, A. and Pal, S.K. (2009). A Versatile Fiber-Optic Coupled System for Sensitive Optical Spectroscopy in Strong Ambient Light. *Rev. Sci. Instrum.*, 80: 053109.
- [85] Bora, T., Kyaw, H.H., Sarkar, S., Pal, S.K. and Dutta, J. (2011). Highly efficient ZnO/Au Schottky barrier dye-sensitized solar cells: Role of gold nanoparticles on the charge-transfer process. *Beilstein J. Nanotechnol.*, 2: 681–690.
- [86] Hu, L., Yan, J., Liao, M., Wu, L. and Fang, X. (2011). Ultrahigh External Quantum Efficiency from Thin SnO<sub>2</sub> Nanowire Ultraviolet Photodetectors. *Small*, 7: 1012–1017.
- [87] Fang, X., Bando, Y., Liao, M., Gautam, U.K., Zhi, C., Dierre, B., Liu, B., Zhai, T., Sekiguchi, T., Koide, Y. and Golberg, D. (2009). Single-Crystalline ZnS Nanobelts as Ultraviolet-Light Sensors. *Adv. Mater.*, 21: 2034–2039.